Optical MEMS: From Micromirrors to Complex Systems

Olav Solgaard, Asif A. Godil, Roger T. Howe, *Fellow, IEEE*, Luke P. Lee, Yves-Alain Peter, *Senior Member, IEEE*, and Hans Zappe

***Abstract*— Microelectromechanical system (MEMS) technology, and surface micromachining in particular, have led to the development of miniaturized optical devices with a substantial impact in a large number of application areas. The reason is the unique MEMS characteristics that are advantageous in fabrication, systems integration, and operation of micro-optical systems. The precision mechanics of MEMS, microfabrication techniques, and optical functionality all make possible a wide variety of movable and tunable mirrors, lenses, filters, and other optical structures. In these systems, electrostatic, magnetic, thermal, and pneumatic actuators provide mechanical precision and control. The large number of electromagnetic modes that can be accommodated by beam-steering micromirrors and diffractive optical MEMS, combined with the precision of these types of elements, is utilized in fiber-optical switches and filters, including dispersion compensators. The potential to integrate optics with electronics and mechanics is a great advantage in biomedical instrumentation, where the integration of miniaturized optical detection systems with microfluidics enables smaller, faster, more-functional, and cheaper systems. The precise dimensions and alignment of MEMS devices, combined with the mechanical stability that comes with miniaturization, make optical MEMS sensors well suited to a variety of challenging measurements. Micro-optical systems also benefit from the addition of nanostructures to the MEMS toolbox. Photonic crystals and microcavities, which represent the ultimate in miniaturized optical components, enable further scaling of optical MEMS. [2013-0297]**

***Index Terms*— Micro-optics, tunable optics, microlenses, micromirrors, optofluidics, photonic crystals, microcavities.**

I. Introduction

OPTICS AND photonics have benefited greatly from miniaturization through MicroElectroMechanical Systems (MEMS). Optical MEMS is a focus for extensive research into the fundamentals of optical interactions because it enables the application of silicon fabrication technology to micro-optical systems and because it provides a unique set of tools for scientific measurements across a wide range of disciplines, making it a driver for the commercial development of optical systems. This paper chronicles the status of research in optical MEMS, starting with a concise history to provide context and then describing research at the forefront of optical MEMS in tunable elements, telecommunications biology and biomedicine sensors, and nanostructures.

The paper is dedicated to Professor Richard S. Muller for his service as a founding director of the Berkeley Sensor & Actuator Center, as the Editor-in-Chief of JMEMS over more than two decades, and for his many contributions to MEMS and optical MEMS.

II. MEMS and Optics: A Concice History

Much of the early work on optical applications of Micro-ElectroMechanical Systems (MEMS) was inspired by sensors and actuators developed in suspended thin films. The fabrication of suspended microstructures by selective etching of patterned, thin films began with the demonstration of an air-gap silicon transistor with a resonant metal cantilever gate by a group led by Harvey Nathanson at Westinghouse Research Labs in the mid-1960s [1]. Optical applications of this technology in the form of projection displays based on micromachined two-dimensional spatial-light modulators emerged in the early 1970s [2]. These early devices and systems led to the development and commercialization of the Digital-Mirror-Device (DMD) [3], [4] by Texas Instruments. However, the mainstream of research and commercialization of MEMS in the 1960s and 1970s focused on the use of single crystal silicon as a microstructural material, with anisotropic etching of the silicon substrate and doped etch-stop layers being the key micromachining process [5]. By the 1970s, researchers were using silicon etching to form microstructures from thin-film materials. At General Motors Research, James Jaffe and John Seto invented a pressure sensor incorporating a diaphragm made of undoped polysilicon protected by a silicon etch-resistant layer [6]. Kurt Petersen at IBM selectively etched an epitaxial silicon layer to release a composite SiO_2-Au cantilever beam for use as a microrelay [7]. The epitaxial layer thickness defined the electrostatic actuation gap between a buried diffusion electrode and the suspended cantilever. Richard Muller and his graduate student Richard Jolly at Berkeley showed that several types of SiO_2-doped silicon composite cantilevers could be released simultaneously using an anisotropic etch of the silicon substrate [8].

The use of polycrystalline silicon (poly-Si) as a structural material in a surface-machining process arose in the context of a specific application: a gravimetric organic-vapor sensor

Manuscript received September 21, 2013; revised March 18, 2014; accepted March 26, 2014. Date of current version May 29, 2014. Subject Editor C. Rembe.

O. Solgaard and R. T. Howe are with the Department of Electrical Engineering, Stanford University, Stanford, CA 94305 USA (e-mail: solgaard@stanford.edu; rthowe@stanford.edu).

A. Godil is with AG Microsystems, San Jose, CA 95054 USA (e-mail: asif@agmicrosystems.com).

L. P. Lee is with the Department of Bioengineering, University of California at Berkeley, Berkeley, CA 94720 USA (e-mail: lplee@berkeley.edu).

Y.-A. Peter is with Ecole Polytechnique de Montréal, Montréal, QC H3T 1J4, Canada (e-mail: yves-alain.peter@polymtl.ca).

H. Zappe is with the Department of Microsystems Engineering, University of Freiburg, Freiburg 79110, Germany (e-mail: zappe@imtek.uni-freiburg.de).

Color versions of one or more of the figures in this paper are available online at http://ieeexplore.ieee.org.

Digital Object Identifier 10.1109/JMEMS.2014.2319266

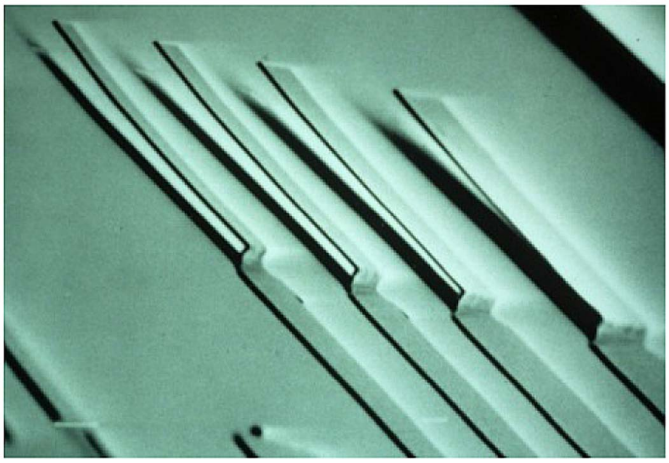

Fig. 1. SEM of 800 nm-thick poly-Si cantilevers fabricated using a 1.5 μm-thick oxide sacrificial layer [9].

using a resonating cantilever [9]. Using an electrostatically driven and sensed cantilever was attractive, especially in view of reproducibility and leakage problems with sputtered ZnO piezoelectric films available in Berkeley's Microfabrication Laboratory at that time [10]. By contrast, poly-Si was routinely deposited using low-pressure chemical-vapor deposition for use in MOSFET gates. It was well known that hydrofluoric acid etched SiO_2 highly selectively with respect to silicon, making it an ideal sacrificial layer. For use in the resonant vapor sensor, a low-loss structural material was needed for the vibrating beam. Although the mechanical properties of poly-Si had not been studied, it was plausible that the grain boundaries would not significantly degrade its elastic properties. Co-fabricating the poly-Si beam with NMOS interface electronics appeared much easier than did the alternative approach of using a sacrificial epitaxial silicon layer [9]. The promise of an integrated, smart sensor – one that fully exploited the accelerating microelectronics revolution – was a major motivator for research in the silicon sensor community.

The initial experiments in 1981 verified that the combination of undoped LPCVD poly-Si for the structural material, a sandwich of thermal and LPCVD SiO_2 for the sacrificial layer, and buffered HF for the release etch was a promising surface micromachining technology [11]. The results from the release of the first set of cantilever beams contained hints of some of the hurdles to making this a practical fabrication process. The cantilevers curved away from the substrate, as shown in Fig. 1, which was attributed to "an internal bending member which is plausible as the result of nonuniform internal stress in the poly-Si layer." [11]. The control of residual stress gradients in poly-Si thin films was the focus of research at a number of laboratories through the next fifteen years. Henry Guckel and his group at the University of Wisconsin discovered that the average stress was tensile, if the deposition temperature was low enough that the film's texture was fine-grained rather than columnar [12]. Some of the longer, thinner cantilevers were observed to adhere to the substrate after release [13], a phenomenon later called "release stiction." Although annealed 400 μm-long cantilevers were successfully released, the authors cautioned that "these results

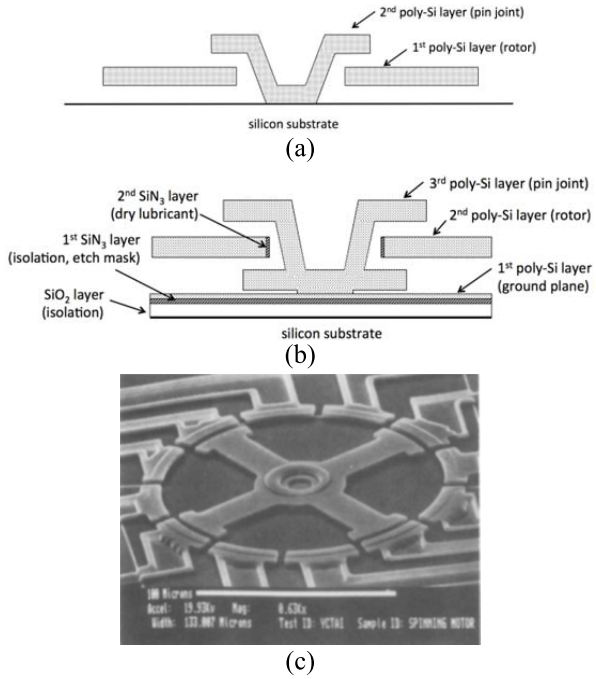

Fig. 2. (a) Cross section of a simple poly-Si pin joint (after [16]). (b) Cross section of a poly-Si micromoto's self-aligned bearing that incorporates substrate isolation, electrical contact through the ground plane, and S_{i3N4} sidwall dry lubricant layer (after [21]). The released rotor is shown halfway between the upper and lower limit stops of the pin joint for clarity in both (a) and (b). (c) Scanning electron micrograph of a poly-Si surface micromachined, variable capacitance electrostatic micromotor using the self-aligned bearing illustrated in Fig. 2(b). The rotor is 120 μm in diameter [22].

are process-dependent and therefore should be considered as first-order guidelines." [13] Finally, the conformal deposition of poly-Si, as seen by its coverage of the near-vertical step in the sacrificial oxide layer Fig. 1, would later become a key feature of the technology.

The co-fabrication of polymer-coated poly-Si resonant cantilevers – including underlying drive and sense electrodes, and NMOS transistors – required an 11-mask process sequence [14]. The principal challenge was to develop a passivation for the transistors and aluminum interconnects during the 40-minute release etch in buffered HF. The mask set with the resonant vapor sensor included a hot-bridge anemometer [15], indicating the potential for poly-Si surface-micromachining technology to support a wide variety of devices.

By the mid-1980s, research groups at Berkeley, Bell Labs and MIT were exploring how poly-Si surface micromachining could be used to fabricate more-sophisticated mechanisms, such as bearings and linkages. The key idea was to use an additional sacrificial and structural layer, which could be patterned to make a simple pin or sliding joint to constrain the motion of a fully-released poly-Si structure (Fig. 2a) [16], [17]. Conformal coverage was an important advantage of poly-Si as a structural material, which is shown by the single-crystal silicon rotors in ref. [17] that are not fully constrained by the "open" pin axle. In the oral presentation of [17], the authors presented several poly-Si mechanisms, such as the gripper later published in ref. [18]. These mechanisms incorporated fully

constrained pin joints made from additional sacrificial oxide and structural poly-Si depositions.

Much of the motivation for exploring poly-Si mechanisms was the possibility of actuating them with electrostatic fields. In contrast to magnetic actuation, the scaling of electrostatic energy densities with decreasing dimensions is favored – even at atmospheric pressure – due to deviations from the large-gap breakdown field for gaps less than a few micrometers. Design studies of electrostatic micromotors indicated the feasibility of side-drive, variable capacitance architectures, for drive voltages in the range of 100 V [19], [20]. The realization of these motors required more-sophisticated bearings than the basic pin joint in Fig. 2a in order to minimize the contacting surface area while providing electrical contact to the rotor. The successful microbearing design illustrated in cross section in Fig. 2b makes creative use of multiple conformal depositions of LPCVD poly-Si, sacrificial oxide and isolation Si_3N_4 layers to fabricate a self-aligned pin joint that suspends the rotor off the underlying poly-Si ground plane [21], [22]. Figure 2c is an SEM of a 120 μm-diameter electrostatic micromotor using this bearing design [22].

The impressive videos of rotating micromotors stimulated great interest in the potential of poly-Si micromechanics at research funding agencies and amongst the general public around the world. In 1987-1988, the National Science Foundation held a series of three workshops to help shape the research agenda for the emerging field of "Microdynamics" [23]. The second workshop was held during the *IEEE Micro Robots and Teleoperators Workshop* in November 1987. At a dinner meeting during that workshop, the organizers decided that "Micro Electro Mechanical Systems" or MEMS was a better name for the field and that the following workshop in February 1989 would be known as *IEEE MEMS*. At that meeting, researchers from Berkeley reported on a large-displacement electrostatic actuator known as the comb drive, which was initially limited to lateral excitation of suspended structures [24].

One of the potential applications of poly-Si micromotors and mechanisms mentioned during this period was optical shutters, with the optical signal entering through an aperture etched through the silicon substrate [20]. However, applications in free-space optics were initially limited by the lack of a surface relief in the essentially flat poly-Si mechanical structures, such as the micromotor in Fig. 2c.

The demonstration of out-of-plane hinged structures in 1991 by K.S.J. Pister and collaborators at Berkeley was a significant breakthrough – one that liberated poly-Si MEMS from the plane of the substrate [25]. This new technology enabled free-space optical components, such as actuated mirrors (Fig. 3) [26], [27] and corner-cube reflectors [28]. These "pop-up" structures were initially fabricated in multilayer (typically three or four layers) poly-Si processes developed at Berkeley, and later at MCNC in the first poly-Si micromachining foundry, the Multi-User MEMS Process (MUMPS), which had its initial run in 1993 [29]. MUMPS and the five-layer poly-Si SUMMiT foundry by Sandia National Labs [30] in 1997 standardized versions of the technology and opened up poly-Si surface micromachining to a broad range of designers.

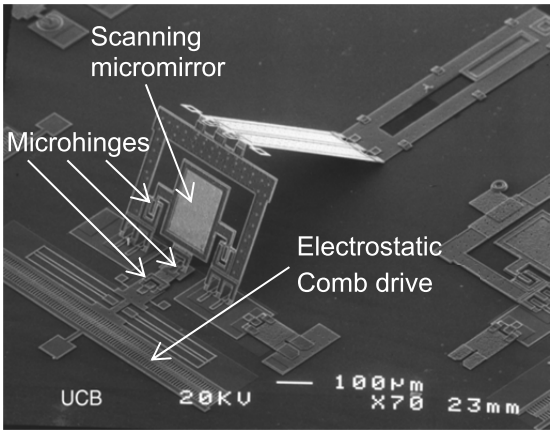

Fig. 3. "Pop-up" poly-Si microscanner. Microhinges allow the scanner to be raised out of plane, and they provide the linkages that connect the combdrive to the scanner. Scanner characteristics: Size - 200 µm by 250 µm, angular range - 30 degrees optical, resonance frequency - 3 KHz.

III. MEMS Tunable Optical Elements

A. MEMS and Micro-Optics

The early work on MEMS-actuated optics, combined with the long traditions and capabilities of classical optics, has led to the development of a very rich discipline of tunable micro-optics [31]. By using microfabrication techniques to manufacture microscale lenses, mirrors, filters, and other types of optical structures, the field of micro-optics has made available a broad spectrum of ultra-miniaturized optical devices. The combination of these with MEMS has, however, expanded the functionality and applicability of these components even further, primarily by making them tunable. We discuss a few examples of these MEMS tunable optical elements in this section.

1) Tuning Micro-Optics: A "tunable" optical component or system is one in which the optical characteristics may be controllably changed; the parameters to be tuned may include focal length, magnification, beam direction, spectral composition, or a host of other factors. In macroscopic optics, this tuning typically requires mechanical motion of one or more elements with respect to others, but in micro-optics entirely new means for optical tuning become possible. These result from the fact that in micro-optics, materials such as liquids, polymers, soft elastomers or flexible semiconductors, to name a few, are employed, using structures and technologies that have no analogs in macro-optical systems.

These novel materials and technologies imply that optical elements may be tuned by changing the characteristics of the components themselves [32]. As we shall see in a few examples below, combining MEMS technology with micro-optics means that microlenses may change their curvature, micromirrors accurately shift their reflection angle, or microfilters change their transmission wavelength, all by altering the optical properties of components on the microscale.

2) The Role of MEMS: Two aspects of MEMS play an important role in the realization of tunable micro-optics. The first is MEMS fabrication technology itself, since micro-optical structures are manufactured using microtechnology, not

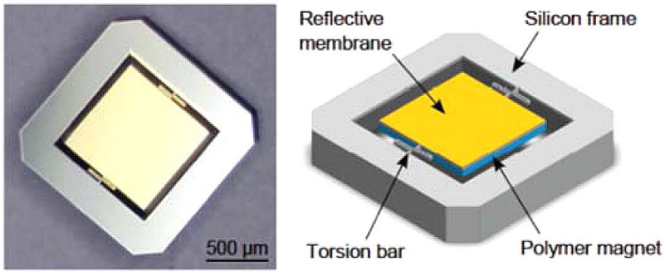

Fig. 4. A hard magnetic micromirror using a polymeric magnet attached to the back side of the tiltable mirror; the mirror and frame are fabricated in silicon [46, Fig. 4].

the traditional production means for macroscopic optics. The formidable arsenal of MEMS cleanroom technologies has been used to realize most of micro-optics, tunable or otherwise, as we know it [33].

The second role of MEMS in tunable optics is the generation of means to actuate tunable components. Whereas the field of optical MEMS initially relied strongly on electrostatic actuation for mechanical movement or positioning of micro-optical components [34], the spectrum of actuation techniques has greatly expanded. Pneumatic, fluidic, thermal, magnetic and even chemical mechanisms for optical tuning have been employed, thus greatly expanding the repertoire of conceivable tunable optical systems.

B. Tunable Micromirrors

Actuated micromirrors are perhaps the oldest micro-optical devices fabricated using MEMS techniques [35], and since they were used from the start as a means to variably deflect an optical beam, they may be considered the "original" tunable micro-optical component. Movable micromirrors with high positioning and attitude accuracy have been made using myriad designs, and served as early demonstrators for the successful combination of micromechanics and micro-optics. As a result, micromirrors have been applied to a wide range of applications in areas as diverse as optical telecommunications [36] and consumer electronics [37], thus representing an optical MEMS success story.

1) Electrostatic Actuation: As MEMS technology has advanced, the spectrum of mirror concepts has likewise broadened and these have become firmly established in the MEMS device repertoire [38], [39]. Whereas the optics of the mirror are relatively simple, one area on which considerable research effort has been expended is actuation for achieving angular and translational movement. Many original concepts used electrostatic actuation, which was shown to be suitable for precise positioning and thus accurate beam steering with a resolution of 0.2° in a scan range of 20° [40]. When combined with micromechanical hinge structures for the mirrors, the typically planar electrostatic actuators were also employed to generate out-of-plane mirror movement [35] for more flexible three-dimensional motion. In addition to possessing positioning accuracy, high-speed actuation was shown to be suitable for video-rate scanning of optical beams [41]; alternatively, large travel range, in excess of 350 μm, could be reached using electrostatic vibromotors [42].

2) Magnetic Actuation: As MEMS technologies have developed, numerous other principles have become feasible for micromirror actuation. Magnetic actuation using silicon and magnetic polymers, as shown in the example of Fig. 4, has led to angular deflections at resonance of $\pm 10°$ for fields of only 0.07mT. Alternatively, purely metallic (nickel) micromirror-based scanners, which do not require expensive SOI substrates for fabrication, have also been shown to provide excellent performance, yielding deflections of $\pm 7°$ for fields of 0.23mT [43]. Magnetically actuated mirrors do not require the high voltages of most electrostatic concepts, and they only require low magnetic fields that can be generated using integrated or ultra-miniaturized coils.

3) Thermal Actuation: Thermal actuators have also been used in a variety of micromirror configurations, including vertically-actuated mirrors for adaptive optics with 6 μm stroke [44]. Using bimorph flexures, which are actuated thermally and rely on residual stress incorporated into the supporting beams during fabrication, several micrometers of vertical mirror motion have been demonstrated in two-dimensional arrays with over 95% fill factor [45], the latter parameter of considerable interest in wavefront control applications.

4) Pneumatic Actuation: As an interesting alternative, the structures and techniques of microfluidics, also an offshoot of MEMS, have led to pneumatically actuated optical components [47], including mirrors and lenses (we discuss the latter in Section III-C2). Using gas-filled microfluidic chambers attached to cavities over which flexible polymer membranes are stretched, increase in gas pressure results in a distension of the membrane, typically in the vertical direction. Using silicon micromachining to generate micromirrors attached to these membranes, the pressure-based distension results in vertical or angular mirror motion. Mirror tilt angles of up to 75 μm and purely vertical motion of 80 μm have been demonstrated using on-chip integrated heaters for thermo-pneumatically actuated devices [48].

C. Tunable Fluidic Optics

Fluidics has become increasingly important for advanced micro-optics. The combination of MEMS fabrication techniques, controlled-liquid configurations and optics has led to the concept of optofluidics, a broad spectrum of technologies, in which fluids and photons play a dominant role in micro-optofluidic systems [49], [50].

Optofluidics has attracted considerable attention due to its utility in realizing new types of displays [51] but has also seen interesting applications in tunable lateral (in-plane) lensing structures [52], tunable photonic crystals [53], and fluidic lasers [54]. We will briefly consider here optofluidics for tunable micro-optical components, in particular lenses and apertures.

1) Liquid Lenses: Liquid droplets on a surface make excellent spherical lenses. It has been shown that the curvature, and thus focal length, of these lenses can be controlled using electrowetting, an electrically-induced change in the liquid contact angle [55], and this concept has been extensively used to realize tunable microlenses

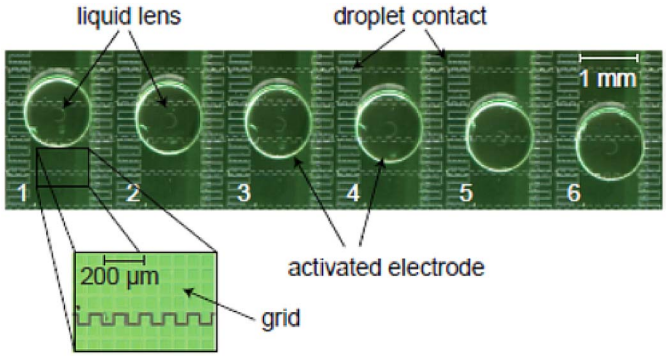

Fig. 5. An electrowetting-actuated repositionable liquid microlens moving in the vertical direction; when in position, its focal length can subsequently be tuned [60, Fig. 17].

[56]. Using micromachining to define placement structures, individual tunable lenses with a stable lateral position and a tuning range between 2.3mm and infinity with less than 50V driving voltage have been demonstrated [57]. Alternative approaches using the dielectrophoretic effect, which requires the application of non-uniform electric fields, have also been employed, albeit with a smaller tuning range [58].

Also possible with electrowetting actuation are tunable lenses with reconfigurable position [59]. As is seen in the example of Fig 5, a liquid microlens is accurately positioned on a structured substrate; once in the correct position its focal length may then also be tuned. In the structures shown, a positioning accuracy of 70 μm and a focal length tuning range of 580 μm to 1,240 μm was demonstrated.

2) Pneumatic Membrane Lenses: An alternative to purely liquid lenses, in which surface tension defines the curvature, is the use of membrane-based lenses, actuated pneumatically. Using the same technology as employed in Section III-B4 for actuating micromirrors, the distended membrane covering a fluid-filled cavity forms a pressure-tunable refractive surface [61], [62]. Pneumatic tuning allows the generation of convex, planar and concave profiles in the same lens, and yields a correspondingly large tuning range; the lack of required electrical power means that lens structures like this are ideal for use in medical or endoscopic imaging, for which high voltages present challenges. Alternatively, completely integrated pneumatic lenses, with on-chip thermal actuation [63], allow compact tunable lens systems with no required pneumatic connections.

The technologies of MEMS also allow realization of more complex optical arrangements using the membrane lens approach. Combining two independently tunable lenses, a zoom system with a zoom ratio of 2.8 in a compact, 18mm-long optical system, has been demonstrated [64]. Furthermore, the use of custom liquids, with well-defined refractive index and dispersion properties, allows the realization of tunable achromatic doublet lenses, which are continuously corrected for chromatic aberration throughout the tuning range [65]. These structures combine classical micromachining with silicone, rather than silicon, materials.

3) Fluidic Apertures: In addition to lens structures, optofluidics has also proven to be of value in generating novel, high-performance tunable apertures and shutters. Rather than using liquids to define refractive surfaces, these devices employ opaque and transparent liquids, which are switched using electrowetting and other microfluidic techniques. The optofluidic shutter of Figure 6 uses a highly absorbing ink, which is alternately switched into and out of the circular aperture [66]. This completely integrated device, requiring only electrical contacts, demonstrated switchable attenuation of 47 dB with switching times below 100 ms; the only moving parts were the two liquids, one absorbing and the other transparent.

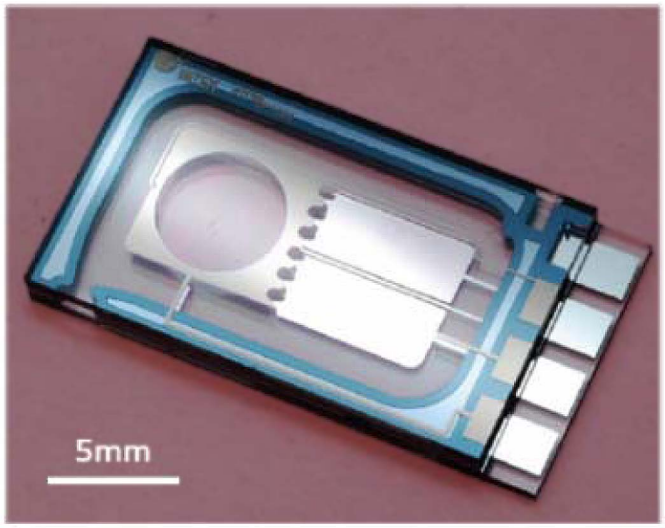

Fig. 6. An optofluidic shutter after chip dicing and prior to liquid filling; an opaque liquid is pumped into and out of the circular aperture using electrowetting.

The attenuation concept can be refined further through the realization of a tunable iris, shown in Figure 7, which allows variable attenuation of an optical beam, again using only moving opaque and transparent liquids [66]. Using circular electrode arrays, the aperture could be opened and closed in four discrete steps with response times in the range of several hundred milliseconds. Using index-matched transparent fluids in this fully-integrated design, transmission characteristics in the open parts of the aperture showed highly uniform transmission with very low wavefront distortion.

D. Tunable Systems

A further advantage of MEMS-based tunable optics, beyond compact tuning mechanisms, which become viable on the microscale, is that microsystems fabrication processes may also be applied to construct tunable systems of considerable mechanical and optical complexity. Such systems may consist of large-scale two-dimensional arrays of tunable lenses, each independently actuated [68], where microfabrication techniques assure good uniformity, high fill factors and compact dimensions not achievable with classical optics manufacturing approaches.

On the other hand, MEMS-based processes, particularly those underlying the concept of the silicon optical bench, allow the assembly of complex systems including tunable lenses, mirrors and shutters [70]. One such example is

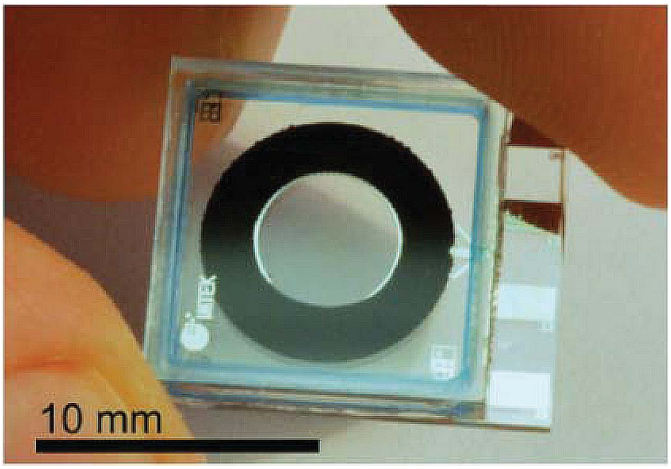

Fig. 7. A fully integrated prototype optofluidic micro-iris in its fully open setting; when actuated, the black opaque liquid moves inward in four discrete steps [67, Fig. 8].

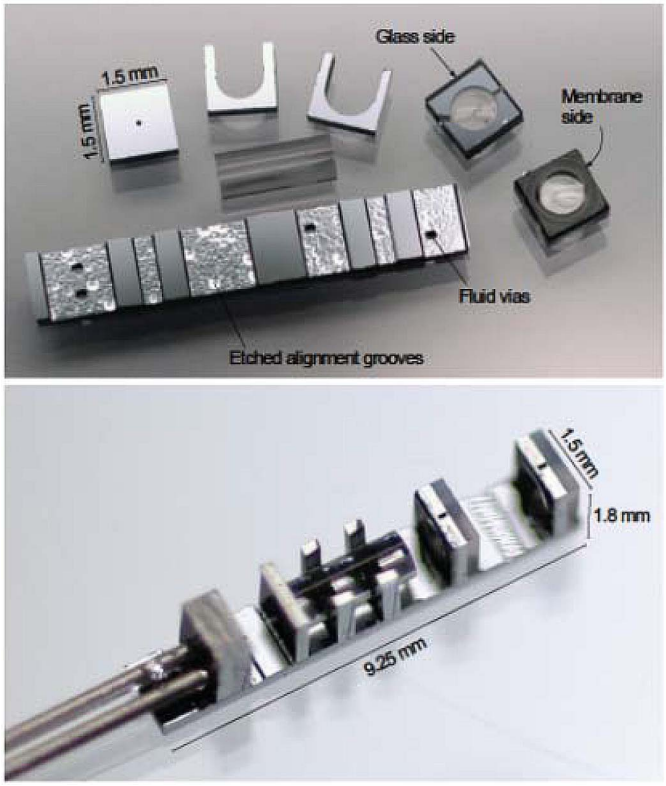

Fig. 8. An optofluidic micro-bench assembled from individually microfabricated components (top) into a system with two independently tunable pneumatic microlenses on a silicon optical bench (bottom) [69, Fig. 2].

shown in Fig. 8: the system includes two independently pneumatically tunable lenses mounted on a silicon substrate machined to allow precision optical alignment and containing the necessary microfluidic channels for actuation as well as fixed-focus GRIN lenses. More-advanced systems include scanning micromirrors, rotational micromotors, and tunable fluidic irises, all to allow three-dimensional imaging with a system whose size scale permits integration into a rigid 3mm endoscope.

These technologies illustrate the possibilities for optical microsystems that become accessible when combining microoptics with MEMS. As microsystems materials and technologies (especially polymers and printing concepts) further mature, the capabilities and application regimes of tunable optical components will likewise expand.

IV. Telecommunications

Optical MEMS has made a huge impact in the field of Optical Networking in the last 15-20 years, particularly in Telecommunication networks. With the increasing demand for more internet data and higher access speeds, Optical Networks play a crucial role in the backbone of the Global Communications Infrastructure. Optical Network providers find themselves constantly in need of cutting-edge technology and innovation that can grow bandwidth at lower cost.

Optical MEMS is a key part of this technology, which allows more dynamic functionality in the physical optical layer and enables a new class of Dynamic Components. Dynamic Components constitute a new breed of device that complements traditional active components (lasers, detectors, modulators) and passive components (multiplexers, isolators, circulators, couplers). First-generation dynamic components have historically included motor-controllable variable optical attenuators (VOAs) and bulk mechanical switches. These early dynamic components did not meet the requirements for integration and compactness. However, dynamic components using Optical MEMS now include optical crossconnects, wavelength selective switches, space switches, VOAs, gain equalizers, channel equalizers, tunable filters and lasers, dynamic dispersion control, and programmable optical add/drop multiplexers.

A technology platform for Dynamic Components, referred to as Diffractive MEMS (DMEMS), was developed at Lightconnect and led to several commercial products. The DMEMS platform uses the wave aspect of light, interference and diffraction. The basic technology, originally referred to as deformable grating modulators, was developed at Stanford University in the early 1990s [71]. The Stanford approach was further developed at Silicon Light Machines for display applications and is shown in Fig 9 below. In the Stanford approach, long narrow ribbons made of silicon nitride (SiN) are suspended above a silicon substrate. The surface is covered with Al or Au to provide an optically reflective surface. In the relaxed state the device looks like a mirror and the light is reflected back. During operation a voltage is applied to every other ribbon, which creates an electrostatic force moving the ribbons downward. This effectively creates a grating, and the incident light is diffracted outside the numerical aperture of the optical system. This approach was useful for display applications, but had serious limitations when applied to fiber-optic applications: large polarization and wavelength dependencies.

The problem was solved by designs that eliminated polarization dependence and significantly reduced wavelength dependence. The device structure (Fig. 10) is a two-dimensional grating structure, in which the suspended membrane is made out of SiN and moves down with electrostatic force as the voltage is applied. The round islands are

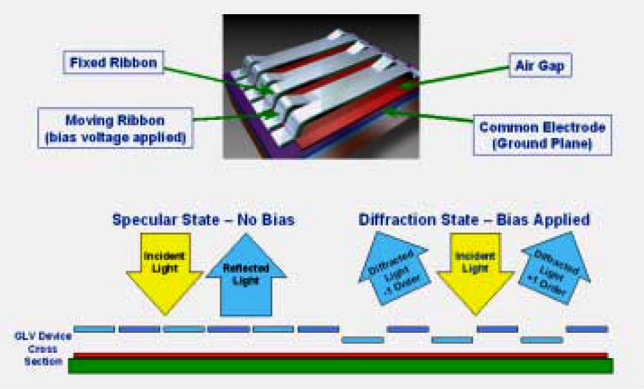

Fig. 9. Deformable grating modulator as developed at Stanford and Silicon Light Machines.

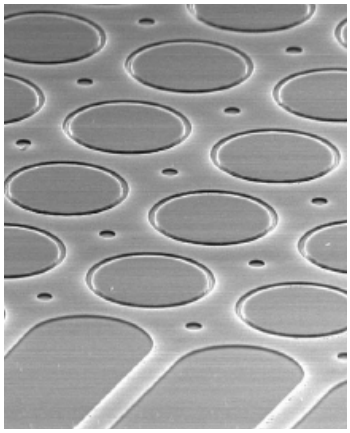

Fig. 10. DMEMS chip from Lightconnect showing 2D grating structure with improved polarization and wavelength dependence. The SiN membrane moves around the fixed islands.

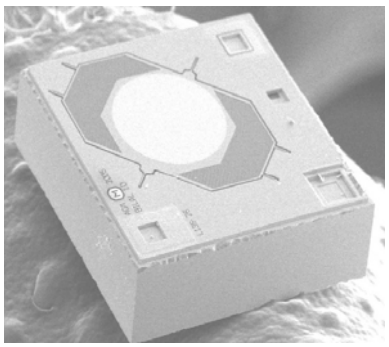

Fig. 11. 1.8 × 1.8 mm MEMS VOA chip from AGM with comb drive and parallel plate actuation.

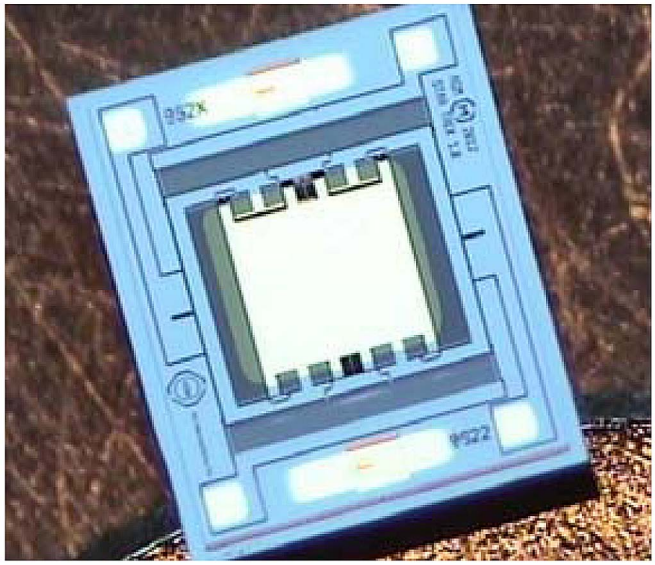

Fig. 12. A 2-axis MEMS Micromirror from AGM for 1 × N switch application.

fixed to the substrate. The four-fold rotational symmetry eliminates polarization dependence. The wavelength dependence is solved by a third reflecting surface on the device that cancels the first wavelength dependence [72]. The product was commercially introduced as a Variable Optical Attenuator (VOA).

The diffractive MEMS approach is not suitable for applications where the light needs to be completely turned off with >45 dB attenuation. MEMS micromirrors are well suited for that and other applications related to switching. AG Microsystems (AGM) has developed a MEMS micromirror chip for a VOA combining comb drive with parallel plate actuation. This offers superior performance at <5V drive and includes protection from overdrive and snapping. The chip (Fig. 11) is able to meet telecommunication requirements on optic performance, on ability to withstand mechanical shock and vibration, and on operating temperature range, and has a lifetime expectancy of 25 years.

The other area of significant interest is switches. This includes wavelength selective switches (WSS) as well as 1 × N and N × N space switches [73]. In a WSS [74] the input light is dispersed with a grating, and the wavelength channels are focused onto a Micromirror array typically comprising 100 micromirrors. The individual wavelength channels can then be switched to different output ports. Significant advances have been made in the WSS and are being commercially deployed in high volume. Recently two-axis micromirrors actuated with comb drives were demonstrated for confocal microscopy [75]. AGM is extending such ideas for developing two-axis micromirrors for space switches such as 1 × N and N × N, including very large cross-connects. A MEMS chip for building 1 × 12 switches is shown below in Fig. 12.

V. Biology and Biomedicine

The initiation of optical MEMS for biomedical applications was accomplished by Dickensheets and Kino [76]. In this work, they demonstrated a miniature scanning confocal microscope that utilizes an off-axis grating as the focusing objective lens and micromachined torsional scanning mirrors to realize real-time confocal imaging with a working distance of 1 mm and an effective N.A. of 0.24 (Fig. 13).

Later Kwon *et al.* demonstrated a three-dimensional raster scanning module that fit into 1 mm^3 as a key part of a micro confocal imaging array for biological lab-on-a-chip applications [77]. In this module, low voltage and large static displacement vertical actuators are integrated with microlenses

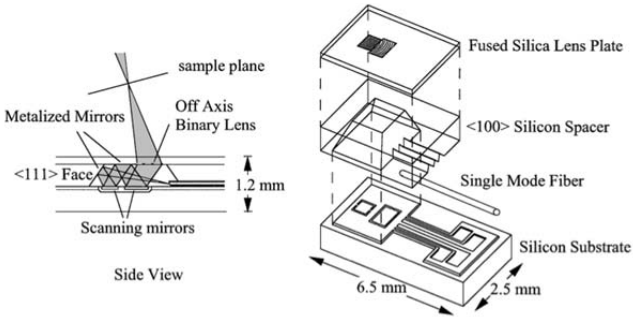

Fig. 13. Micromachined confocal scanning microscope, consisting of a single-mode optical fiber for illumination and detection, two tortional mirrors for scanning, and a binary transmission grating as the objective lens.

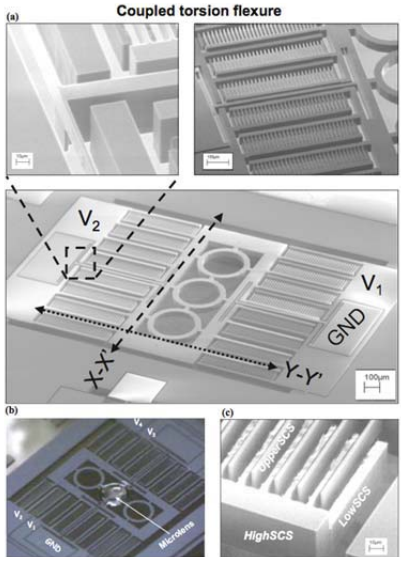

Fig. 14. SEM and picture of fabricated vertical microlens scanner: (a) SEM of unidirectional device, (b) Microscopic picture of bi-directional device with polymer lens, (c) Self aligned vertical comb fingers.

on high-aspect-ratio silicon-on-insulator (SOI) structures. The unique isolated vertical comb drives and the coupled-torsion flexures provide upward and downward piston motion with low driving voltages (Fig 14).

As shown in Fig 15, Kwon *et al.* established an isolation method for SOI MEMS technologies and demonstrated vertical comb-drive-based two-dimensional gimbaled MEMS scanners with large static rotation [78]. These twoaxis optical MEMS mirrors are useful in biomedical imaging, raster scanning and image projection. This method of backside island isolation provides electrical isolation as well as mechanical coupling of SOI structures without additional dielectric backfill and planarization. It allows a gimbal structure with electrical isolation, enabling two-axis rotation of MEMS scanners for biomedical imaging applications.

The first miniature scanning confocal microscope with electrostatically actuated microlenses for focusing and scanning was demonstrated in 2003 (Fig. 16). In this microscope, the objective lenses, scanners, pupil, and pinhole of the confocal microscope are integrated in a volume smaller than 2 mm^3 [79]. The objective lenses are composed

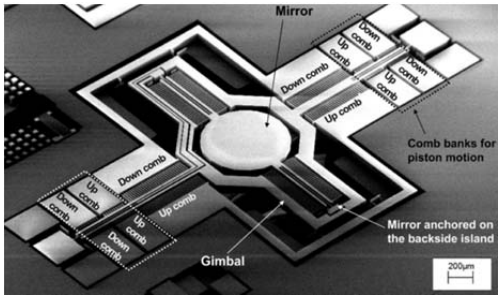

Fig. 15. SEM of 2D MEMS scanner for biomedical imaging applications.

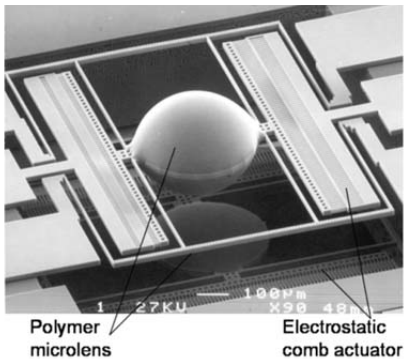

Fig. 16. Scanning electron micrograph of MEMS microlens scanners. Two microlens scanners are orthogonally aligned and vertically stacked together.

of two vertically cascaded polymer microlenses integrated onto micromachined comb actuators. Raster scanning is implemented by electrostatically actuating each microlens in orthogonal directions. The system achieved reflection confocal imaging with 3 μm transverse resolution over a 100 Single Molecule μm field of view and a 0.38 mm working distance at $\lambda = 633$nm. This device demonstrates the combination of silicon micromachining, polymer micromachining, and vertical stacking of different substrates.

In 2007, Ra *et al*. demonstrated a two-dimensional MEMS scanner for dual-axis confocal microscopy (Fig. 17) [80]. They fabricated the scanner by using a double SOI wafer that enabled actuation by self-aligned vertical electrostatic comb drives. Maximum optical deflections of $\pm 4.8°$ and $\pm 5.5°$ are achieved in static mode for the outer and inner axes, respectively. This team achieved reflectance images with a field of view of 344 μm $\times$ 417 at 8 frames/s. The transverse resolutions are 3.94 and 6.68 μm for the horizontal and vertical dimensions, respectively. As a result, they demonstrated real-time high-resolution *in vivo* imaging with their two-dimensional MEMS scanner.

Ra *et al*. also presented a handheld dual-axis confocal microscope (Fig. 18) [81]. The fully packaged microscope has a diameter of 10 mm and acquires images at 4 Hz frame rate with a maximum field of view of 400 μm $\times$ 260 μm. The transverse and axial resolutions of the handheld probe are 1.7 μm and 5.8 μm, respectively. The capability to perform real time small animal imaging is demonstrated *in vivo* in transgenic mice.

These optical MEMS components enable biomedical applications such as optogenetics and noninvasive endoscopic

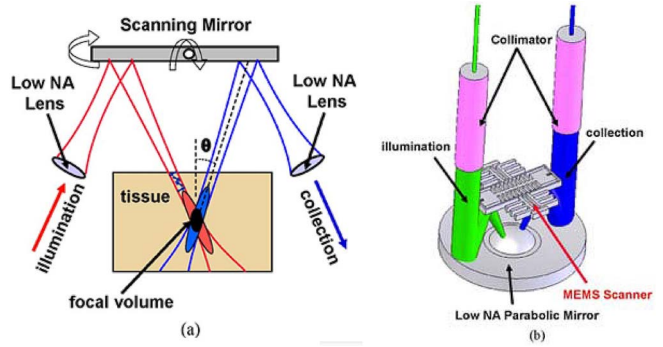

Fig. 17. (a) Dual-axes confocal microscopy principle. (b) Schematic of endoscopic probe.

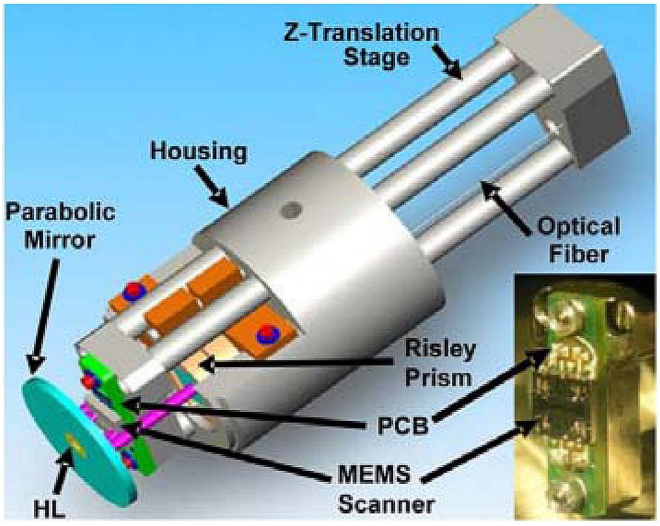

Fig. 18. Schematic of a 10 mm diameter handheld probe with the packaged MEMS scanner in the inset.

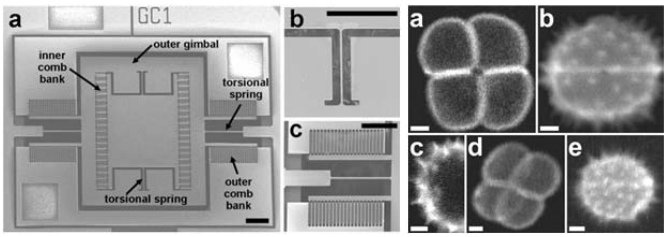

Fig. 19. Left: Scanning electron micrograph of the MEMS scanner; overall scanner design (a), detail of torsional spring (b), and detail of outer comb banks. Right: Two-photon fluorescence images of pollen grains acquired using instrumentation based on a MEMS scanner (a-e) ([82], Fig 1 & 3).

screening for disease, etc. For example, a group at Stanford demonstrated a fast-scanning two-photon fluorescence imaging based on optical MEMS, which has the acquisition rates of lines up to ~3.5 kHz (Fig. 19).

The Stanford group also established a miniature microendoscope, which consists of a combination of the MEMS scanning mirror, microlenses and fiber-optic technology (Fig. 20). The microscope is sufficiently small that an adult mouse can carry the 2.9-gram device on its head while allowing the microscope to capture deep brain images of awake and moving animals.

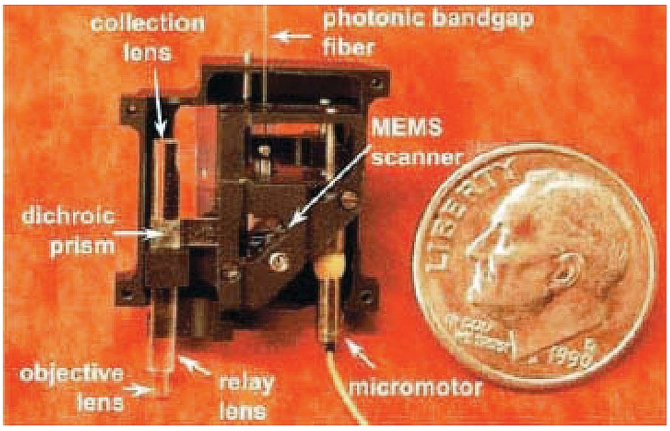

Fig. 20. Miniature microendoscope, which consist of a combination of a MEMS scanning mirror, microlenses, and fiber-optic technology.

A. Optical MEMS: Single Molecule Detection

The ultimate goal of most bioMEMS systems is to monitor biological processes with sensitivity, selectivity and good temporal resolution. Current advanced Optical MEMS/NEMS enables the miniaturized tools that are used to investigate individual bio molecules to achieve high precision and throughput. One of the first attempts to investigate single-molecular-level detection was made by Seo *et al* [83]. As in Fig. 21, they utilized integrated Si_xN_y microfluidic devices with microelectrodes to achieve a bondless nano- to microfluidic interface, low transmission loss and good stability under challenging external environmental parameters such as rapidly changing temperature and the presence of corrosive gasses. They demonstrated detection of a single 500 nm size florescent bead and fluorescently-labeled DNA. Autonomous biophotonic MEMS without a conventional microscope was achieved by designing single-layer-based two-dimensional optical scanners. Following this development many similar MEMS designs were realized for the detection and manipulation of single biological entities [84].

Significant progress in single-molecule detection with Optical MEMS has been achieved in the genomic sequencing field. Pacific Biosciences has developed a next-generation DNA sequencer based on a zero-mode wave-guide system, which provides extreme optical confinement and enables singlenucleotide sensitivity while DNA polymerase constructs the sequence as shown in Fig. 22. The principle of this NanoElectroMechanical System (NEMS) is straightforward and simple. All waveguides have a specific cut-off wavelength beyond which propagation cannot be sustained. At wavelengths longer than the threshold, the field decays exponentially along the propagation direction resulting in an evanescent wave [85]–[87]. The practical decay length comprises zeptoliter observation volumes within the guide for ultra-sensitive biomolecular detection.

B. Optical MEMS and Microfluidics: Optofluidics

The optofluidics field has combined flexible microfluidic systems with tunable optical MEMS/NEMS and advanced

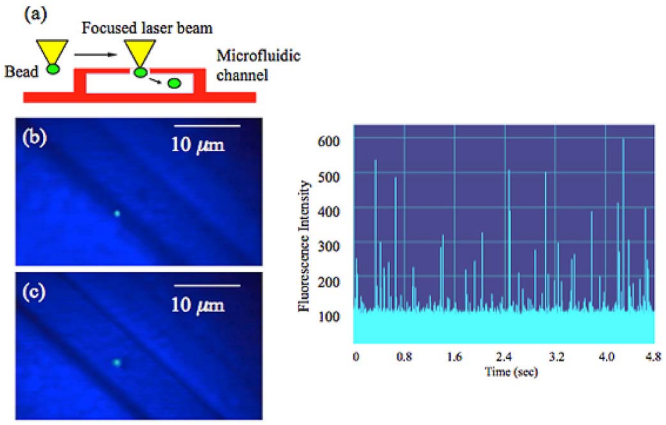

Fig. 21. Biophotonic MEMS for single molecule detection and manipulation. Left: (a) cross sectional diagram of silicon nitride microfluidic system with integrated micropores; (b) 500 nm fluorescent beads trapped outside of microfluidic channels; (c) 500 nm fluorescent beads transported from outside the microfluidic channels to the inside by optical trapping; Right: Detection of single carboxy-rhodamine 6G molecules excited with a 488 nm Ar laser and detected by an APD.

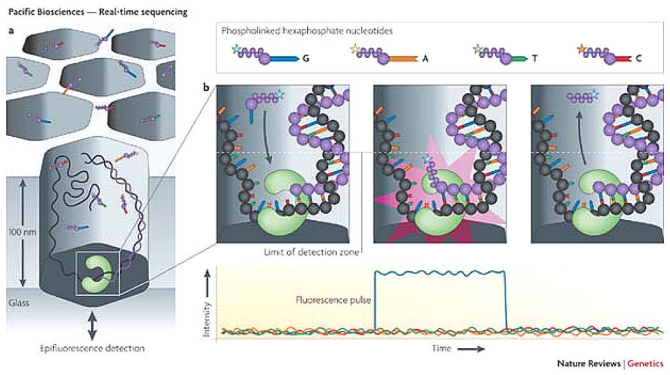

Fig. 22. MEMS implementation of a four-color real-time sequencing platform is shown. Zero-mode waveguides provide ultra-compact detection volume allowing high signal-to-noise detection.

optics to create lab-on-a-chip instruments, biomolecular sensors and molecular-imaging tools [88]. Integration of photonic circuits plays a key role for devices that are more functional and compact [89]. In addition to optical sensing, active biological manipulation has been achieved utilizing both optical and non-optical forces, including hydrodynamics and dielectrophoresis (DEP). This dual-purpose use of optics (actuation and detection), makes optofluidics a very attractive approach to biomedical instrumentation that requires biomolecular manipulation and observation.

Liu *et al.* demonstrated the use of optofluidics to control photothermal nanoparticles [90]. Their work was based on direct optical-to-hydrodynamic energy conversion using suspended photothermal nanoparticles near the liquid–air interface utilizing submilliwatt power. They were able to drive and guide liquid flow in microfluidic channels to transport biomolecules and living cells at controlled speeds and directions (Fig. 23). This work laid the foundation for optically driven, large-scale optofluidic circuits for biomolecular sensing and manipulation.

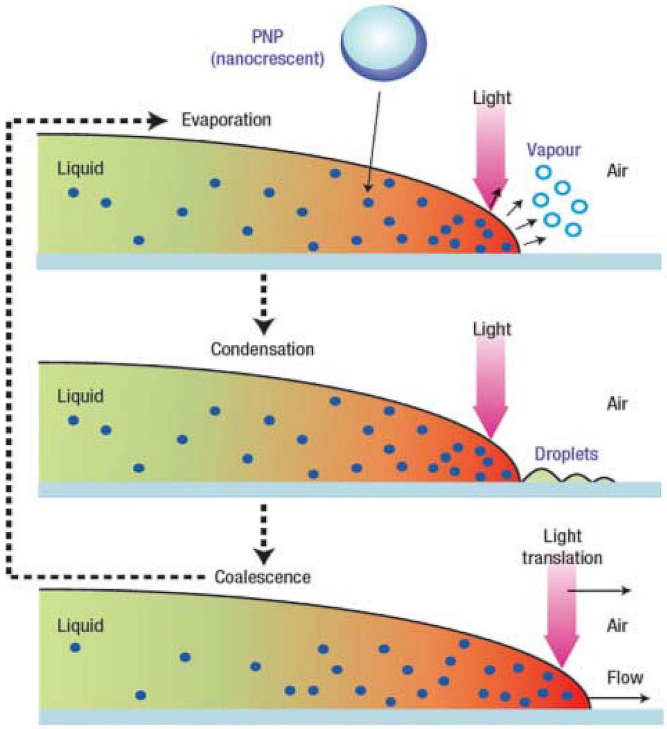

Fig. 23. Photothermal Nanoparticle (PNP)-activated optofluidic flow. The main principle of the optically controlled advance of the liquid–air interface and its experimental applications are shown.

As shown in Fig. 24, Yang *et al.* demonstrated active DNA manipulation (λ-DNA) by creating stronger optical confinement and higher intensities than those of diffraction-limited systems [91]. Their technique simultaneously utilizes near-field optical forces to restrain matter inside the waveguide and scattering/adsorption forces for transport. Lien *et al.* demonstrated optofluidic integration with eight solid-core waveguides to observe fluorescent particles [92].

A similar concept with metal-clad, dynamically-reconfigurable liquid lenses in a microfluidic channel was demonstrated by Tang *et al.* [93]. Figure 25 shows a schematic diagram of the device and how it focuses light from an optical fiber through the liquid lens. The lens is formed by three laminar liquid flows that interact to create the desired refractive-index profile in the region where the lens forms.

In addition to biomolecules such as DNA, RNA, and proteins, a larger biological entity – Caenorhabditis elegans (C. elegans) – has been investigated using microfluidics with embedded low-cost and high-resolution microscopy [94]. Figure 26 shows the implementation and application of a high-resolution, lensless and fully on-chip microscope system. Utilizing either gravity-driven flow or electrokinetic flow for positioning yields a compact, low-cost imaging solution.

A variety of optical interactions enable various biological/medical applications such as Surface Enhanced Raman Spectroscopy (SERS) as in the microfluidic platform in Fig. 27 [95]–[97]. A very promising approach is to use optofluidic resonators for SERS signal amplification within micro- or nanofluidics. Various biological molecules, including Dengue

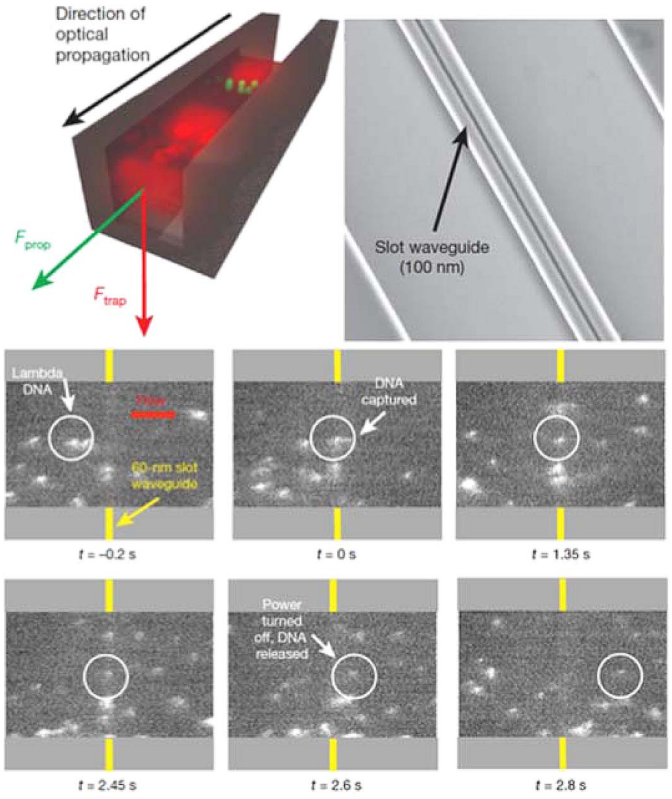

Fig. 24. Schematic of an optofluidic device for active particle manipulation. Consecutive images display individual YOYO-tagged λ-DNA trapped over an optically excited 60-nm-wide slot waveguides.

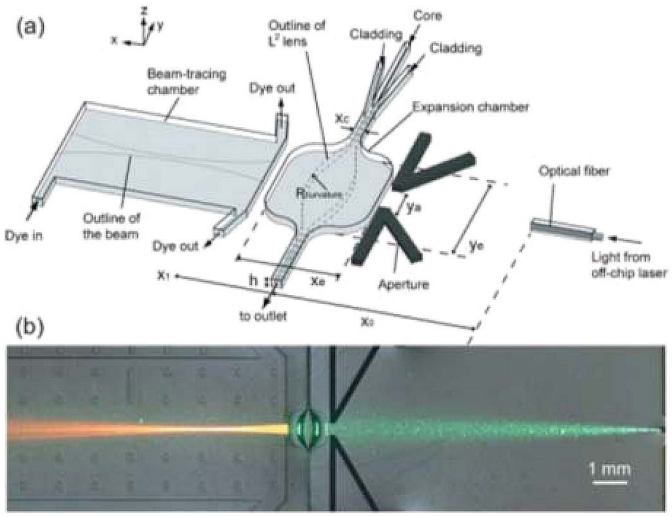

Fig. 25. (a) Schematic of the principle of operation of a reconfigurable microfluidic liquid lens. (b) Experimental implementation of beam focusing.

virus and Aβ protein, have been targeted for maximum signal amplification by SERS.

Taking advantage of the amplification ability of SERS and implementing a miniaturized immunoassay, Lee *et al.* [98], presented a programmable and fully automatic gold array-embedded gradient microfluidic device for providing a convenient and reproducible surface-enhanced Raman scattering (SERS)-based immunoassay platform for cancer

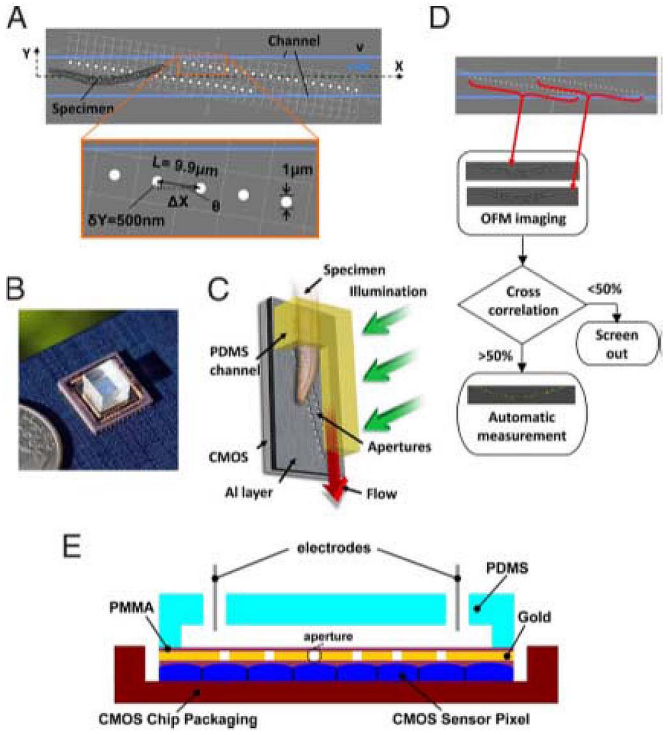

Fig. 26. OFM (Optofluidic Microscopy) prototype. Top view (a), package (b), schematic design (c), operational steps (d), and cross section (e) are illustrated.

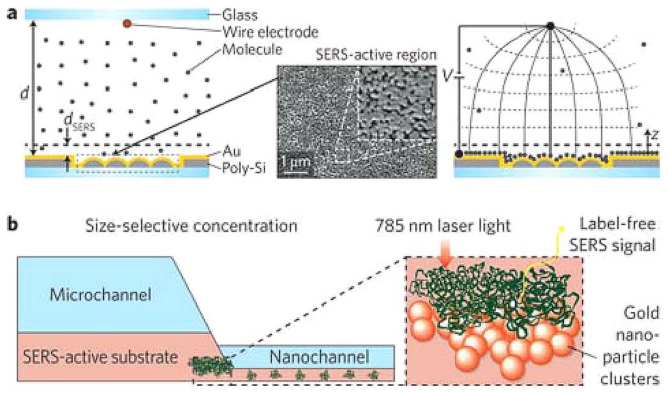

Fig. 27. (a) Electrokinetic concentration of analyte molecules at the SERS-active surface in a microchannel. (b) Size-selective detection of protein aggregates using a nanofluidic channel.

biomarkers as shown in Fig. 28. They achieved automatic serial dilution by the gradient microfluidic generator and a total analysis time less than 60 minutes.

Micro-optofluidics also enables particle synthesis. Sunghoon Kwon and his group at the Seoul National University developed a technique that can synthesize free-floating microstructures in microfluidic channels at the desired time and location within the field of view of the lithography system [99], [100]. Figure 29 shows a detailed procedure of Kwon's maskless particle-generation system. They demonstrated a real-time in-situ polymerization process to dynamically synthesize extruded polymeric microstructures with various two-dimensional shapes. They used high-speed spatial light modulators to dynamically control

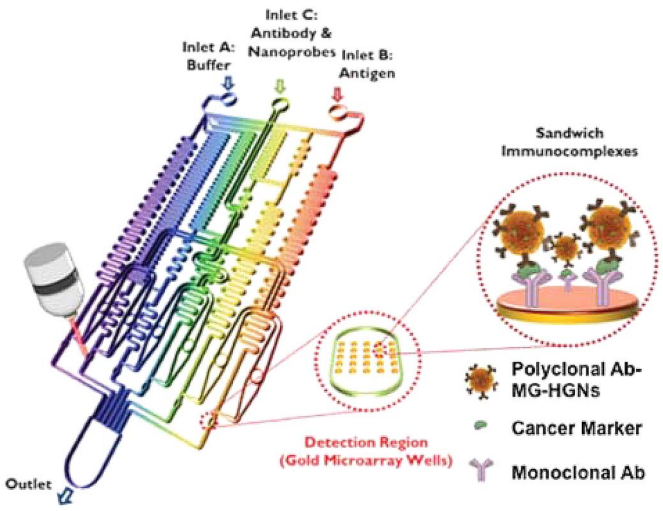

Fig. 28. Schematic of gold array-embedded gradient chip for SERS-based immunoassays.

shapes of polymerized microparticles and to achieve high throughput.

The Institute for Optofluidics and Integrated Nanophotonics (IONAS) has developed reconfigurable optofluidic nanophotonic circuits, which are promising in applications such as optical information processing and highly sensitive and localized optical sensing [101]–[103]. They have investigated optofluidic PhC microcavities (Fig. 30) and their properties in the context of (bio) sensing. High quality factors of the order of 6×10^4 have been demonstrated.

VI. Sensors

Sensors represent the canonical MEMS application, to the point that MEMS in the early years was seen as synonymous with sensors and actuators. That tradition also plays a big part in the development of Optical MEMS: Optics provides new functionality to MEMS sensors, and MEMS technology enables scaling of optical sensors. The results are sensors that combine the precision, low noise and electromagnetic interference (EMI) immunity of optical measurements with the compactness and flexibility of MEMS to enable a wide range of sensor applications.

Most Optical MEMS sensors are based on some type of optical interferometer. Interferometers can be classified into two groups: multiple-beam interferometers with finite time response and recirculating interferometers with infinite time response. Fig. 31 shows typical examples of these two types of interferometers and explains their operational principles.

In the Michelson (or the Mach-Zehnder, which is the unfolded version of the Michelson), the input beam is split into two paths by a non-polarizing beam splitter. After having propagated along the two different paths through the interferometer, the two beams are recombined in the same beam splitter. In the Fabry-Perot, the input optical field is coupled to the optical cavity through the front mirror, and then the incoupled field circulates back and forth inside the cavity with a characteristic photon lifetime given by the mirror reflectivities and the cavity

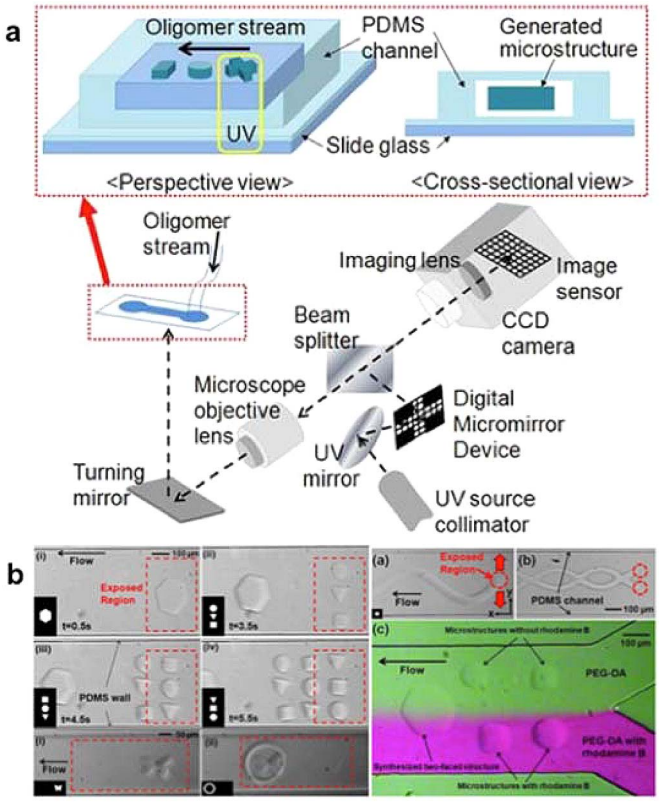

Fig. 29. (a) Schematic diagram of optofluidic maskless lithography system. (b) Dynamic control using optofluidic maskless lithography.

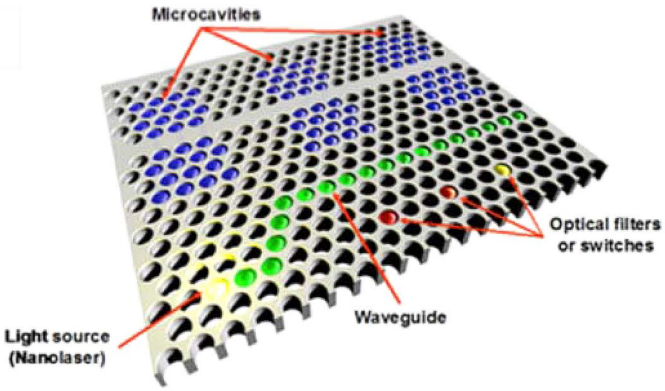

Fig. 30. Schematic representation of a reconfigurable optofluidic photonic crystal circuit. The basic platform is a planar photonic crystal structure with air holes.

losses. The total reflected light and transmitted light through the FP is determined by the phase of the recirculating fields in the cavity.

On resonance, the recirculating fields add in phase on the output of the resonator, and all the light is transmitted and none is reflected, due to the fact that the light reflected from the front mirror is out of phase with the recirculating fields at the front mirror. This leads to the characteristic FP's response to mirror separation. Two cavity types are shown. In the first, the mirror reflectivities are high (r=0.98) and there are no cavity losses except the mirrors. The transmission is then sharply peaked around the mirror separations that lead to

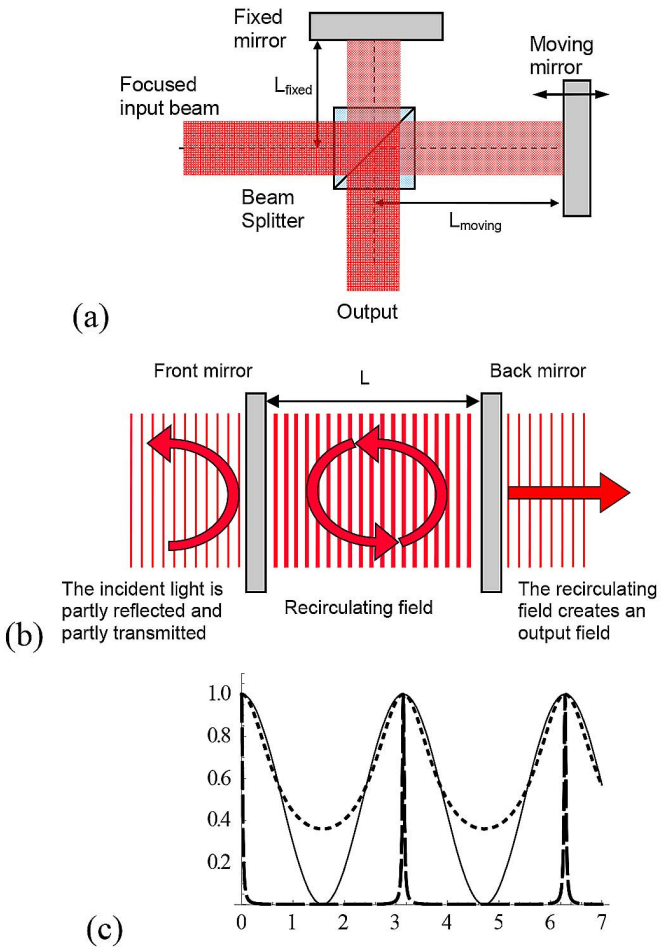

Fig. 31. (a) The Michelson interferometer is a two-beam interferometer, in which the light is split into two paths that after some propagation distance are recombined. (b) In the Fabry-Perot interferometer, the input field recirculates inside the cavity, and the transmission and reflections are determined by the phase relationships of the recirculating fields at the mirrors. (c) Transmission as a function of mirror separation in two-beam and recirculating interferometers. The solid line represents the response of a two-beam interferometer; short-dashed and long-dashed lines are for FP with field reflectivities of 0.5 and 0.98, respectively.

resonance. The second example shows an FP with relatively weakly reflecting mirrors (r=0.5). The resonance conditions that give total transmittance are unaltered, but the resonances are much broader due the lower photon lifetime in the cavity.

In Fig. 31c, the two different responses of FPs are compared to the response of a two-beam interferometer. The transmission goes to unity at resonance when the fields are in phase at the output, but we now only have two interfering beams, so the response is a harmonic function of the path length difference. These comparisons illustrate the tradeoffs involved in choosing an interferometer structure for an optical MEMS sensor. Fabry-Perot resonators with low loss (i.e. long photon lifetime) give rise to sharply peaked responses that are very sensitive to mirror separation around the resonance condition. That enables very sensitive sensors but also requires high stability and reproducibility of nominal mirror separation and interrogating wavelength. Two-beam interferometers and low-photon-lifetime FPs, on the other hand, give rise to responses that are less peaked and therefore less sensitive, but also less demanding of the stability of the nominal mirror separation and the interrogating wavelength.

Both multiple-beam and recirculating interferometers are common in Optical MEMS. The Grating Light Valve [71] and the Gires-Tornoise interferometer [104] are examples of optical MEMS implementations multibeam interferometers while Fabry-Perot resonators and ring resonators are examples of recirculating interferometers used in Optical MEMS. New sensor applications and new system geometries based on these are constantly being developed.

A. Atomic Force Microscopy (AFM)

Atomic Force Microscopy (AFM) is one of the very successful sensor applications of optical MEMS. The optical lever is by far the most commonly used detection technique for determining the motion of AFM cantilevers. Optical MEMS interferometers have also had significant impact on the development of AFM. By incorporating two-beam grating interferometers into AFM cantilevers, improved force sensitivity and bandwidth can be achieved, which enable new system functionalities.

Figure 32 compares a regular AFM tip whose position is measured by an optical lever and an AFM tip with an integrated high-bandwidth grating force sensor [105], [106]. Both cantilevers utilize an optical lever to measure the harmonic up-and-down motion of the cantilever itself, which is driven on resonance so its motion is close to harmonic. The interdigitated force sensor measures forces applied to the tip by interferometrically detecting the offset between the tip-coupled finger and the reference fingers of the interferometer. The offset between the two sets of fingers leads to a diffraction pattern, of which two orders are picked up on the four-quadrant detector as shown in Fig. 32c. The standard optical lever yields a single optical beam on the four-quadrant detector, while the grating cantilever creates a diffraction pattern as shown. In both cases, the ratio of light detected in quadrants 1+2 to quadrant 3+4 gives the vertical position of the tip. The ratio 1+4 to 2+3 is only used for alignment in the traditional optical lever while the interdigitated cantilever creates a diffraction pattern that depends on the relative position of the interdigitated fingers.

As shown in Fig. 32c, the reflected light (0^{th} order diffraction mode) from the grating is positioned on quadrants 2 or 3, while the 1^{st} order diffraction mode is positioned on quadrants 1 or 4. The relative optical power detected by 2+3 vs. 1+4 therefore allows the calculation of the bending of the tip-coupled fingers.

This improves the AFM in two important ways: the tip-sample force is detected with better force resolution, and the bandwidth of the force measurements is increased due to the high resonance frequency of the tip-coupled fingers. The net result is that the tip-sample force can be measured with improved resolution both in force and time. That allows studies of surfaces at a level of detail and calibration of surface properties that is not possible with standard AFMs.

Figure 33 shows a surface map of the reduced Young's modulus of a copolymer surface in water [107]. The imaged sample is a styrene-ethylene/butylene (SEBS) copolymer that

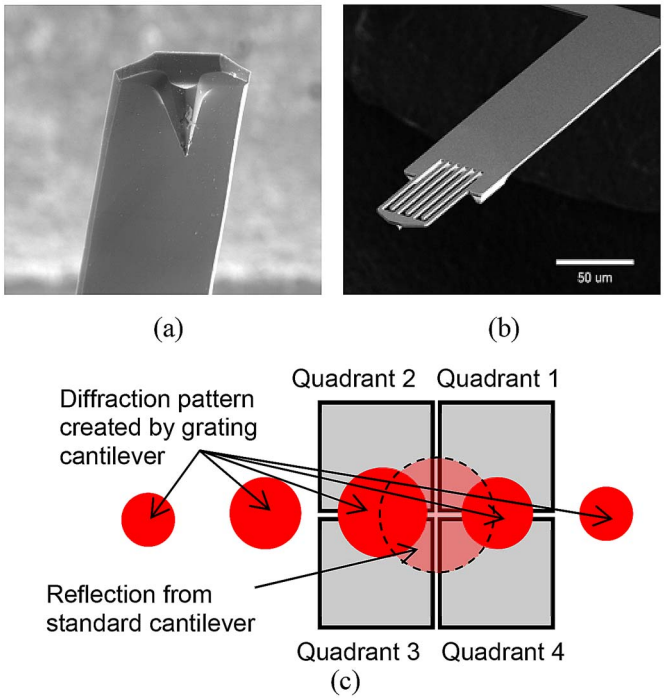

Fig. 32. (a) Atomic Force Microscope cantilever designed for position measurements by an optical lever. (b) AFM cantilever with integrated, interdigitated grating force sensor. (c) Diffraction pattern from an interdigitated cantilever on the four-quadrant detector. Only the 0^{th} order and one of the 1^{st} orders of the diffraction pattern are used.

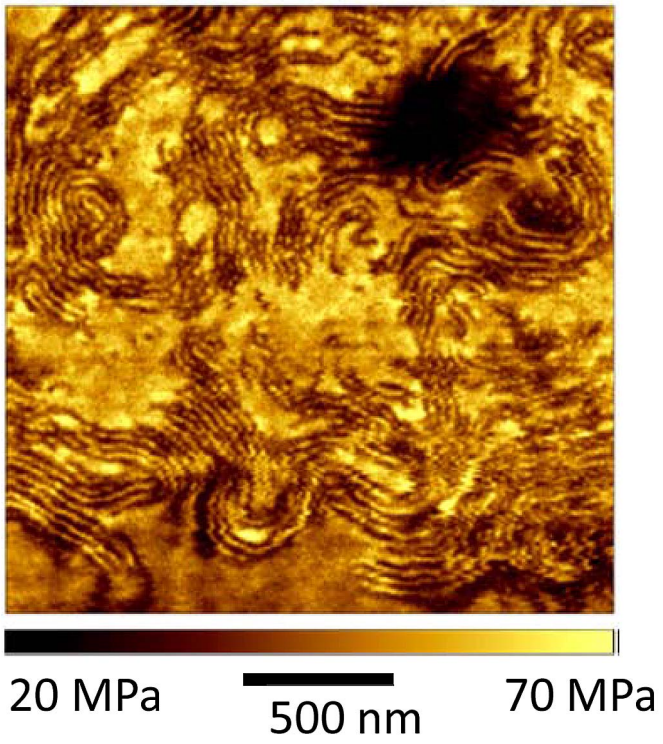

Fig. 33. Reduced Young's modulus of a styrene-ethylene/butylene (SEBS) copolymer submerged in water. The numerical values of the reduced Young's modulus are calculated from the tip-sample interaction force, which has been mapped with high temporal resolution over the surface of the sample.

is composed of a hard polystyrene segment and a softer rubbery segment of poly (ethylene/butylene). Figure 33 clearly shows the characteristic nanoscale lamellar structures of the sample. The reduced Young's modulus is calculated from the time waveform of the tip-sample interaction force that is measured with the grating interferometer. It is particularly significant that the map is obtained in water because numerically calibrated characterizations of surfaces in aqueous solutions open up new avenues for investigations in material science and biology.

B. In-Plane Fabry-Pérot Cavities

Fabry-Pérot interferometers have the potential to be significantly more sensitive than two-beam interferometers and are therefore favored in many optical MEMS sensor applications. In-plane Fabry-Pérot cavities based on Bragg reflectors made of vertically etched high aspect ratio multilayered silicon-air structures (Fig. 34) are attractive for their ease of integration with electrostatic actuators, microfluidic systems, optical fibers and waveguides. However, they present high insertion loss and relatively low finesse due to Gaussian beam divergence and surface roughness at the silicon-air interfaces of multilayered structures [108]. Therefore, telecommunication applications cannot be considered. However, promising applications were reported such as tunable filters [109], sensors [110]–[112] and high quality factor resonators [113].

When attached to one of the Bragg mirrors, a spring-actuator system (Fig. 35) was able to shift the resonance wavelength of the Fabry-Pérot cavity by more than 100nm [109]. When integrated with a fiber laser or a semiconductor optical amplifier, such filters demonstrated tuning of the output wavelength over several tens of nanometers with applications as swept sources for optical coherence tomography [114].

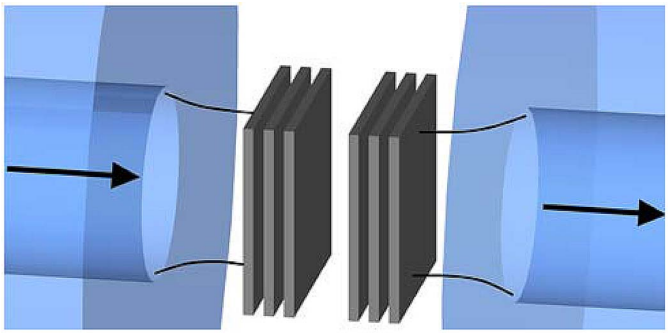

Fig. 34. Schematic representation of a Fabry-Pérot cavity made of two Bragg mirrors of 2.5 silicon-air periods coupled at normal incidence to single-mode fibers.

In-plane Fabry-Pérot cavities are easily integrated with waveguides. They offer a robust integration alternative that was used for the demonstration of an optical accelerometer for spacecraft navigation systems [111]. In this case, one Bragg mirror is attached to a suspended proof mass (Fig. 36).

Integrated sensors are probably the most attractive applications for in-plane Fabry-Pérot cavities. Indeed, they offer simple, compact and robust assembly of several components on chip such as waveguides, proof masses, microfluidic channels and Bragg mirrors. The case of volume refractive index sensing is of particular interest. The rational for measuring the volume refractive index is to be able to measure the cellular refractive index in flow cytometry, thus providing addi-

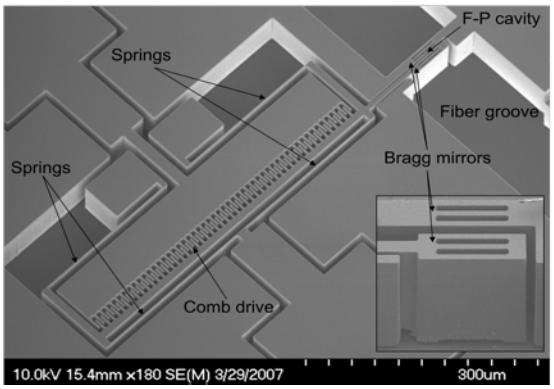

Fig. 35. Scanning electron micrograph of in-plane tunable Fabry-Pérot filter integrated with fiber grooves, springs and electrostatic actuator.

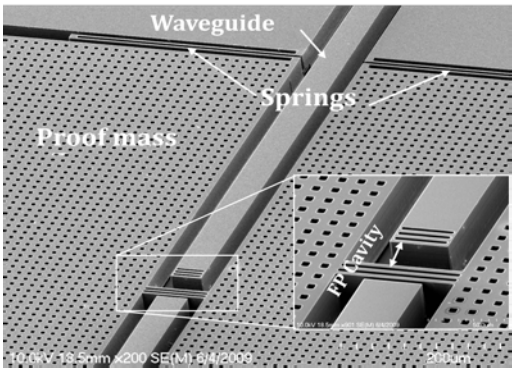

Fig. 36. Scanning electron micrograph of the in-plane Fabry-Pérot accelerometer integrated with waveguides, springs and proof mass.

tional parameters for cell type differentiation. A resolution of 1.7×10^{-5} RIU (refractive index unit) was demonstrated using an in-plane Fabry-Pérot cavity integrated with microfluidic channel (Fig. 37) [110].

A mixed solution of two populations of glass beads having different diameter was statistically differentiated [115]. More recently, Melanoma (B16) and Lymphoma (EL4) cells flowing through the device (Fig. 38) were successfully distinguished [116]. In addition to cell differentiation, this type of device has the capability of identifying cancerous cell populations by measuring their refractive index [117].

Gas sensing can also be realized using in-plane Fabry-Pérot cavities when filled with polymers. In this case, the sensing principle is based on polymer swelling upon gas absorption. The magnitude of the deformation is recorded through the resonance wavelength shift of the on-chip silicon Fabry–Perot interferometer and is proportional to the analyte concentration (Fig. 39). Limits of detection down to the ppm level have been demonstrated [112].

VII. Nanostructures

A. Optical Microcavities

Confinement and manipulation of light in optical microcavities has been the subject of intense fundamental and applied research for more than a decade [118]. Recent advances in micro- and nanotechnology have allowed the realization of small micron-size cavities used in various applications

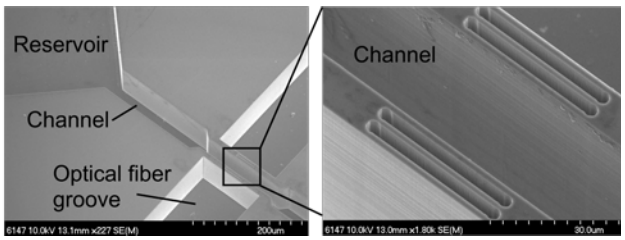

(a) (b)

Fig. 37. (a) Scanning electron micrograph of Fabry-Pérot refractometer integrated with optical fiber alignment grooves, microfuidic channel, and reservoir. (b) Closeup view of the Fabry-Pérot refractometer made of two silicon/air Bragg reflectors separated by the microfluidic channel.

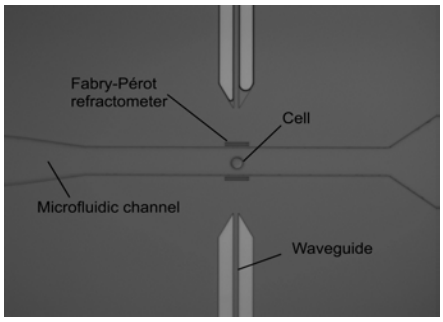

Fig. 38. Photograph of a cell flowing through a Fabry-Pérot refractometer integrated with optical waveguides and microfuidic channel.

such as enhancement of spontaneous emission [119], photon sources [120], filters [121], single-molecule sensors [122], [123], optical frequency combs [124], and optomechanical oscillators [125], [126] to name a few. The main reasons for recent advances are significant improvements in size reduction and surface quality enabled by advanced micro- and nanotechnology processes. The most important figure of merit for optical microcavities is the Purcell factor, which gives the enhancement of spontaneous emission into a given mode of the microcavity with respect to the emission in free space. The Purcell factor is proportional to the quality factor and inversely proportional to the volume of the mode [127]. Thus having near-perfect geometries and surface quality will maximize the quality factor, whereas reducing size will minimize the mode volume. Several optical MEMS have optical microcavities or microresonators in their components. We will present a nonexhaustive list of examples in this section. Mainly two types of optical microcavities will be highlighted: photonic crystals and whispering-gallery-mode resonators.

B. Photonic Crystals

Photonic crystals in one and two dimensions are simple to fabricate and integrate in microsystems. They exhibit guided resonances that can be used for sensing [128], fluorescence enhancement [129] and enhanced reflections [130], and if integrated with microactuators, they can serve as the basis for micromechanically tunable optical sensors and filters [131]–[133].

The development of one-dimensional and two-dimensional Photonic Crystals (PCs), shown schematically in Fig. 40, has also expanded the role of FP sensors. In PF-FP sensors, the PCs act as resonant mirrors. These PCs are interferometers in

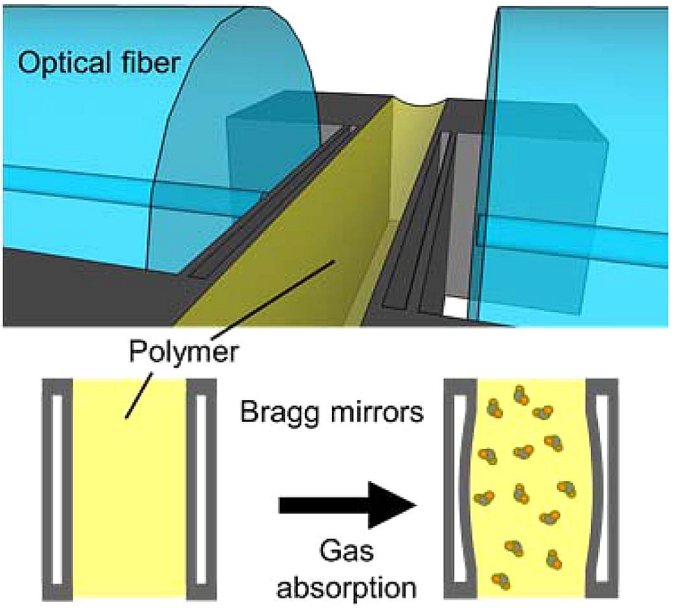

Fig. 39. Schematic of in-plane Fabry-Pérot gas sensor. Schematic representation of the sensor operation principle. Upon gas absorption, polymer expansion deforms the interferometer, inducing a shift of its resonance wavelength.

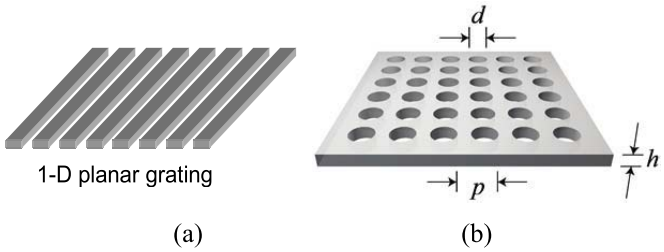

Fig. 40. One-dimensional (a) and two-dimensional (b) Photonic Crystals. The two-dimensional crystal has a square unit cell with circular holes, and it is fully characterized by the pitch (p), hole diameter (d), crystal thickness and the material parameters.

their own right, in addition to being used as building blocks in interferometric systems.

To understand how one-dimensional or two-dimensional PCs act as interferometers, consider Fig. 41. The incident light, shown as a plane wave at normal incidence, will be reflected from the front and back surfaces of the PC and a circulating field will build up in the PC. In this sense the PC slab acts as a FP resonator to define what we call the direct pathway through the crystal. In addition to the direct pathway, the incident light may also couple to guided resonances [134] of the PC. The guided resonances can be thought of as the generalization of the guided modes of a uniform slab. The periodicity of the holes in the PC provides the required phase match that allows these modes, which in the uniform slab are completely guided, to couple to radiation outside the slab. Once the light is coupled into the guided resonances, it is re-radiated with a specific photon lifetime given by the structure of the guided resonance.

The direct and indirect pathways represent two fundamentally different ways for light to propagate through the PC. The incident light is therefore split in two parts that propagate

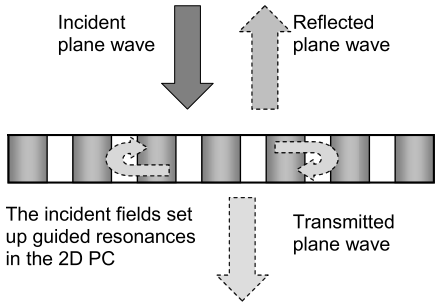

Fig. 41. Transmission through a PC slab is determined by interference between pathways through the crystal. In the direct pathway, the PC acts as a uniform slab of some intermediate index of refraction between the index values of the PC material and the surrounding medium (typically air). In the indirect pathway, the incident light couples to guided resonances, which couple back out in either direction from the slab with a characteristic decay time. The direct and indirect paths interfere to establish reflection and transmission through the PC.

separately through the PC, just like the incident light in the Michelson interferometer of Fig. 31a is split into two paths. Once the light of guided resonance reradiates, it interferes with the directly reflected wave and directly transmitted wave to create the total reflectance and total transmittance. The PC is therefore an interferometer, just like the Michelson or Mach-Zehnder. Notice in particular that the in-plane band gap of the PC plays only an indirect role in determining the transmission and reflection of two-dimensional PCs. It is the presence of a guided resonance, not its absence, that makes the PC behave differently than a simple slab of homogeneous material.

The guided resonances are described by their center frequency, or center wavelength, and their lifetime. The center frequency is most strongly affected by the periodicity of the PC, while the lifetime of an infinite PC is most strongly affected by the scattering strength of the individual unit cells. The scattering is a complex function of the size and shape of the unit cells. In the case of a simple two-dimensional PC, as shown in Fig. 40b, small holes lead to weak scattering and a long lifetime, while the opposite is true for larger holes.

By engineering the characteristic center frequencies and lifetimes of the guided resonances, we can control the interference between the direct and indirect pathways and thereby the reflectance and transmittance of the PC. Short lifetimes give rise to broadband effects that are useful for creating broadband mirrors [130], [135], [136], polarization optics [137], [138], filters [139], and beam splitters. Long lifetimes, on the other hand, create sharp transitions in the reflectance and transmittance spectra [136]. Such transitions are useful for a number of sensor applications [140]–[142] that require narrow band response or precise tracking of spectral features.

The total lifetime of a guided resonance is determined by the in- and outcoupling and by any other loss mechanisms. For small PCs the edge loss, either through scattering or simply through coupling to the slab beyond the PC edge, puts a lower limit on the PC loss, and therefore a higher limit on the lifetime of the guided resonances. This means that broadband PCs are simple to scale to small sizes, while careful attention has to be paid to avoiding edge loss for successful scaling of narrow band PCs.

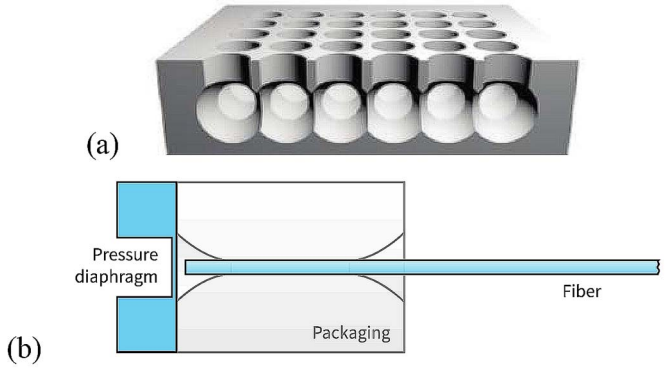

Fig. 42. (a) High reflectivity PC diagraph fabricated in a monolithic film of Si. (b) Fiber optic pressure sensor that utilizes a high reflectivity Si diaphragm as the pressure sensing element.

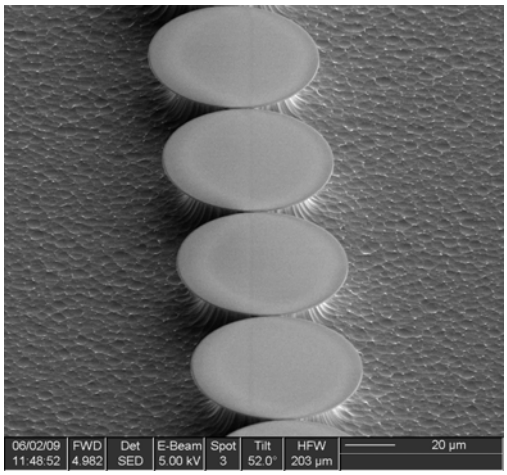

Fig. 43. Scanning electron micrograph of a silica microdisks CROW with 1.1 m gap between cavities.

The literature describes a vast number of ways to fabricate one-dimensional and two-dimensional photonic crystals. Typically, they involve patterning and etching of the PC structure in a thin film of high refractive index, e.g. deposited Poly-Si films, epitaxially grown films, or the device layer in Silicon-on-Insulator (SOI) wafers. To support the guided resonances that give the PC their optical characteristics, the material surrounding the high-index film must have lower refractive index.

One fabrication method that is particularly well suited to integration of PCs into MEMS is the Generation Of PHotonic Elements by Reactive etching (GOPHER) [143], [144]. In this process, the PCs are etched directly into Si using a combination of directional and isotropic etches. The resulting structure is a monolithic PC with a hole array over an isotropically underetched cavity as shown in Fig. 42a. The cavity can be connected in each unit cell as shown, or the array of holes can be completely underetched. The underetched cavity provides the low-index layer that is required to support guided resonances.

The excellent optical and mechanical properties of two-dimensional PC reflectors make them ideal for a number of applications. They have been directly integrated into MEMS scanners [145], and they can be transferred to a variety of substrates through contact printing [133]. Figure 42b illustrates how monolithic Si PC reflectors can be used to create pressure sensors [146], [147]. The pressure-sensing diaphragm in this sensor is the high-reflectivity PC shown in (a), and it provides high sensitivity, due to its excellent optical and mechanical properties, combined with chemical and thermal robustness that far exceeds that of metal and dielectric-stack mirrors.

C. Whispering Gallery Mode Resonators

Whispering-gallery-mode (WGM) resonators have been recently extensively reported either as microspheres, microdisks or microtoroids. Although the highest quality factor up to 10^{10} is reached with crystalline resonators [148], silica is preferred since it has lowest intrinsic material loss. Quality factors as high as 10^8 are achieved with silica [149]. However light coupling to silica optical microcavities is challenging and requires highly sensitive alignment of tapered optical fibers. It is important to note that for such evanescent coupling to a waveguide, the measured quality factor depends on the coupling regime. It is therefore important to know the coupling regime in order to extract the intrinsic quality factor. This can be done through a Stokes parameters analysis [150]. Biosensing [151], [152], optical frequency combs [153] and optomechanics [154] have attracted a lot of attention recently. However, other applications such as coupled-resonator optical waveguides (CROW) and optical microcavities made of chalcogenide glasses are promising alternatives for slow-light and low-threshold sources respectively. CROWs were fabricated from as many as 8 silica microdisks (Fig. 43) [155]. Raman lasing in As_2S_3 high-Q whispering-gallery-mode resonators was recently demonstrated with a threshold as low as 13 μW [125].

Delay time of 109ps was demonstrated [155] with relatively low quality factors (Q~10^4) indicating promise for slow-light generation in CROWs when using high-Q silica resonators. Due to their small mode volume and long photon lifetime, WGM optical microcavities are excellent candidates for nonlinear processes generation. As_2S_3 chalcogenide glass microspheres pumped at 1550nm were used to generate Raman scattering emission at 1634nm [156]. Threshold as low as 13 W with 11% efficiency was demonstrated [120].

VIII. CONCLUSIONS

Micromachining allows the tools of the integrated circuit industry, lithography and parallel processing to be applied to optical devices and systems. The payoff is integration of mechanics, fluidics, magnetics and optics into highly functional microsystems with numerous advantages in terms of functionality, flexibility, stability, sensitivity, size and, ultimately, cost. The application areas for these types of Optical MEMS include tunable optics, spatial light modulators, fiber-optical communication devices and systems, optofluidic systems for biological and chemical analysis, and interferometric sensors. The augmentation of Optical MEMS by nanostructures has led to the development of Optical Nanosystems based on photonic crystals and ultra-compact optical resonators that

are applicable to a wide range of systems across all the sub-disciplines of optics.

ACKNOWLEDGEMENTS

The authors wish to acknowledge the contributions of collaborators too numerous to name. Hans Zappe is grateful to the dedicated Freiburger Micro-opticians, past and present, who have been instrumental in establishing the field of tunable micro-optics. Olav Solgaard is grateful for the dedication and inspiration of his students and colleagues at Stanford, BSAC, SINTEF, University of Oslo, and UC Davis. The field of optical MEMS has seen tremendous developments over the last two decades, and it is not possible to include all relevant references to all the subjects that are discussed. To give a coherent coverage to such a broad field, the authors have discussed and referenced work they are most familiar with in greater detail. The authors acknowledge and apologize for the many omissions that necessarily have resulted.

REFERENCES

[1] H. C. Nathanson, W. E. Newell, and R. A. Wickstrom, "A resonant gate silicon bandpass transistor," in *Proc. IEEE IEDM*, Washington, DC, USA, Oct. 1965, p. 38.

[2] R. N. Thomas, J. Guldberg, H. C. Nathanson, and P. R. Malmberg, "The mirror-matrix tube: A novel light valve for projection displays," *IEEE Trans. Electron Devices*, vol. 22, no. 9, pp. 765–775, Sep. 1975.

[3] L. J. Hornbeck, "Deformable-mirror spatial-light modulators," *Proc. SPIE*, vol. 1150, pp. 86–102, Aug. 1989.

[4] R. M. Boysel, T. G. McDonald, G. A. Magel, G. C. Smith, and J. L. Leonard, "Integration of deformable mirror devices with optical fibers and waveguides," *Proc. SPIE*, vol. 1793, pp. 34–39, Sep. 1992.

[5] K. D. Wise, "Integrated sensors, MEMS, and microsystems: Reflections on a fantastic voyage," *Sens. Actuators A, Phys.*, vol. 136, no. 1, pp. 39–50, 2007.

[6] J. M. Jaffe and J. Y. W. Seto, "Polycrystalline silicon pressure transducer," U.S. Patent 4 003 126, Jan. 18, 1977.

[7] K. E. Petersen, "Micromechanical voltage controlled switches and circuits," in *Proc. IEEE IEDM*, Washington, DC, USA, Dec. 1978, pp. 100–103.

[8] R. D. Jolly and R. S. Muller, "Miniature cantilever beams fabricated by anisotropic etching of silicon," *J. Electrochem. Soc.*, vol. 127, no. 12, pp. 2750–2754, 1980.

[9] R. T. Howe, "An evaluation of surface-acoustic-wave and cantilever-beam oscillators for integrated organic-vapor sensors," M.S. thesis, Dept. Elect. Eng. Comput. Sci., Univ. California, Berkeley, CA, USA, Oct. 1981.

[10] P. Chen *et al.*, "A planar-processed PI-FET accelerometer," in *Proc. IEEE IEDM*, Washington, DC, USA, Dec. 1980, pp. 848–849.

[11] R. T. Howe and R. S. Muller, "Polycrystalline silicon micromechanical beams," in *Proc. Electrochem. Soc. Spring Meet.*, Montreal, QC, Canada, May 1982, pp. 184–185.

[12] H. Guckel, D. W. Burns, C. C. G. Visser, H. A. C. Tilmans, and D. Deroo, "Fine-grained polysilicon films with built-in tensile strain," *IEEE Trans. Electron Devices*, vol. 35, no. 6, pp. 800–801, Jun. 1988.

[13] R. T. Howe and R. S. Muller, "Polycrystalline silicon micromechanical beams," *J. Electrochem. Soc.*, vol. 130, no. 6, pp. 1420–1423, 1983.

[14] R. T. Howe and R. S. Muller, "Integrated resonant-microbridge vapor sensor," in *Proc. IEEE IEDM*, San Francisco, CA, USA, Dec. 1984, pp. 213–216.

[15] Y.-C. Tai, R. S. Muller, and R. T. Howe, "Polysilicon bridges for anemometer applications," in *Proc. 3rd Int. Conf. Solid-State Sens. Actuators*, Philadelphia, PA, USA, Jun. 1985, pp. 354–357.

[16] L.-S. Fan, Y.-C. Tai, and R. S. Muller, "Pin joints, gears, springs, cranks, and other novel micromechanical structures," in *Proc. 4th Int. Conf. Solid-State Sens. Actuators*, Tokyo, Japan, Jun. 1987, pp. 849–852.

[17] K. J. Gabiel, W. S. N. Trimmer, and M. Mehregany, "Micro gears and turbines etched from silicon," in *Proc. 4th Int. Conf. Solid-State Sens. Actuators*, Tokyo, Japan, Jun. 1987, pp. 853–856.

[18] M. Mehregany, K. J. Gabriel, and W. S. N. Trimmer, "Integrated fabrication of polysilicon mechanisms," *IEEE Trans. Electron Devices*, vol. 35, no. 6, pp. 719–723, Jun. 1988.

[19] W. S. N. Trimmer and K. J. Gabriel, "Design considerations for a practical electrostatic micro-motor," *Sens. Actuators*, vol. 11, no. 2, pp. 189–206, 1987.

[20] S. F. Bart, T. A. Lober, R. T. Howe, J. H. Lang, and M. F. Schlecht, "Design considerations for micromachined electric actuators," *Sens. Actuators*, vol. 14, no. 3, pp. 269–292, 1988.

[21] L.-S. Fan, Y.-C. Tai, and R. S. Muller, "IC-processed electrostatic micromotors," in *Proc. IEEE IEDM*, San Francisco, CA, USA, Dec. 1988, pp. 666–669.

[22] Y.-C. Tai and R. S. Muller, "IC-process synchronous micromotors," *Sens. Actuators*, vol. 20, pp. 49–55, Nov. 1989.

[23] K. Gabriel, J. Jarvis, and W. Trimmer, Eds., "Small machines, large opportunities: A report on the emerging field of microdynamics," in *Proc. NSF Workshop Microelectromech. Syst.*, AT&T Bell Laboratories, 1988.

[24] W. C. Tang, T.-C. H. Nguyen, and R. T. Howe, "Laterally driven polysilicon resonant microstructures," in *Proc. IEEE MEMS*, Salt Lake City, UT, USA, Feb. 1989, pp. 53–59.

[25] K. S. J. Pister, M. W. Judy, S. R. Burgett, and R. S. Fearing, "Microfabricated hinges: 1 mm vertical features with surface micromachining," in *Proc. 6th Int. Conf. Solid-State Sens., Actuators, Transducers*, San Francisco, CA, USA, Jun. 1991, late paper in Supp. Vol., pp. 1–4.

[26] O. Solgaard, M. Daneman, N. C. Tien, A. Friedberger, R. S. Muller, and K. Y. Lau, "Optoelectronic packaging using silicon surface-micromachined alignment mirrors," *IEEE Photon. Technol. Lett.*, vol. 7, no. 1, pp. 41–43, Jan. 1995.

[27] M.-H. Kiang, O. Solgaard, R. S. Muller, and K. Y. Lau, "Micromachined polysilicon microscanners for barcode readers," *IEEE Photon. Technol. Lett.*, vol. 8, no. 12, pp. 1707–1709, Dec. 1996.

[28] D. S. Gunawan, L.-Y. Lin, and K. S. J. Pister, "Micromachined corner cube reflectors as a communication link," *Sens. Actuators A, Phys.*, vol. 47, nos. 1–3, pp. 580–483, 1995.

[29] D. A. Koester, R. Mahadevan, and K. W. Markus, *Multi-User MEMS Processes (MUMPs) Introduction and Design Rules*. Research Triangle park, NC, USA: MCNC MEMS Technol. Appl. Center, 1992, p. 39.

[30] J. J. Sniegowski and M. S. Rodgers, "Multi-layer enhancement to polysilicon surface-micromachining technology," in *Proc. IEEE IEDM*, Washington, DC, USA, Dec. 1997, pp. 903–906.

[31] H. Zappe, "Micro-optics: A micro tutorial," *Adv. Opt. Technol.*, vol. 1, no. 3, pp. 117–126, 2012.

[32] C. Friese, A. Werber, F. Krogmann, W. Mönch, and H. Zappe, "Materials, effects and components for tunable micro-optics," *IEEJ Trans. Elect. Electron. Eng.*, vol. 2, no. 3, pp. 232–248, May 2007.

[33] H. Zappe, *Fundamentals of Micro-Optics*. Cambridge, U.K.: Cambridge Univ. Press, 2010.

[34] M. C. Wu, O. Solgaard, and J. Ford, "Optical MEMS for lightwave communication," *J. Lightw. Technol.*, vol. 24, no. 12, pp. 4433–4455, Dec. 2006.

[35] K. Petersen, "Silicon torsional scanning mirror," *IBM J. Res. Develop.*, vol. 24, no. 5, pp. 631–637, 1980.

[36] D. Bishop, C. Giles, and G. Austin, "The Lucent LambdaRouter: MEMS technology of the future here today," *IEEE Commun. Mag.*, vol. 40, no. 3, pp. 75–79, Mar. 2002.

[37] L. Hornbeck, "Current status of the digital micromirror device (DMD) for projection television applications," in *Proc. IEEE IEDM*, Dec. 1993, pp. 381–384.

[38] R. Conant, *Micromachined Mirrors*. Norwell, MA, USA: Kluwer, 2003.

[39] K. Hane and M. Sasaki, "Micro-mirrors," in *Comprehensive Microsystems*, vol. 3, Y. Gianchandani, O. Tabata, and H. Zappe, Eds. Amsterdam, The Netherlands: Elsevier, 2007, ch. 3, pp. 1–63.

[40] N. Tien, O. Solgaard, M. Kiang, M. Daneman, K. Lau, and R. Muller, "Surface-micromachined mirrors for laser-beam positioning," *Sens. Actuators A, Phys.*, vol. 52, no. 1, pp. 76–80, 1996.

[41] R. A. Conant *et al.*, "A raster-scanning full-motion video display using polysilicon micromachined mirrors," *Sens. Actuators A, Phys.*, vol. 83, no. 1, pp. 291–296, 2000.

[42] M. J. Daneman, N. Tien, O. Solgaard, A. Pisano, K. Lau, and R. Muller, "Linear microvibromotor for positioning optical components," *J. Microelectromech. Syst.*, vol. 5, no. 3, pp. 159–165, Sep. 1996.

[43] N. Weber, H. Zappe, and A. Seifert, "An all-nickel magnetostatic MEMS scanner," *J. Micromech. Microeng.*, vol. 22, no. 12, pp. 1250089-1–125008-7, 2012.

[44] P. A. Krulevitch *et al.*, "MOEMS spatial light modulator development at the center for adaptive optics," *Proc. SPIE*, vol. 4983, pp. 172–179, Jan. 2003.

[45] M. A. Helmbrecht, U. Srinivasan, C. Rembe, R. T. Howe, and R. S. Muller, "Micromirrors for adaptive-optics arrays," in *Proc. TRANSDUCERS 2001*, pp. 10–14.

[46] N. Weber, D. Hertkorn, H. Zappe, and A. Seifert, "Polymer/silicon hard magnetic micromirrors," *J. Microelectromech. Syst.*, vol. 21, no. 5, pp. 1098–1106, Oct. 2012.

[47] A. Werber and H. Zappe, "Tunable pneumatic micro-optics," *J. Microelectromech. Syst.*, vol. 17, no. 5, pp. 1218–1227, Oct. 2008.

[48] A. Werber and H. Zappe, "Thermo-pneumatically actuated, membranebased micro-mirror devices," *J. Micromech. Microeng.*, vol. 16, no. 12, pp. 2524–2531, Dec. 2006.

[49] D. Psaltis, S. Quake, and C. Yang, "Developing optofluidic technology through the fusion of microfluidics and optics," *Nature*, vol. 442, pp. 381–386, Jul. 2006.

[50] Y. Fainman, L. Lee, D. Psaltis, and C. Yang, Eds., *Optofluidics*. New York, NY, USA: McGraw-Hill, 2010.

[51] J. Heikenfeld *et al.*, "Electrofluidic displays using Young–Laplace transposition of brilliant pigment dispersions," *Nature Photon.*, vol. 3, pp. 292–296, Apr. 2009.

[52] X. Mao, J. Waldeisen, B. Juluri, and T. Huang, "Hydrodynamically tunable optofluidic cylindrical microlens," *Lab Chip*, vol. 7, no. 10, pp. 1303–1308, 2007.

[53] D. Erickson, T. Rockwood, T. Emery, A. Scherer, and D. Psaltis, "Nanofluidic tuning of photonic crystal circuits," *Opt. Lett.*, vol. 31, no. 1, pp. 59–61, 2006.

[54] D. Vezenov, B. Mayers, D. Wolfe, and G. Whitesides, "Integrated fluorescent light source for optofluidic applications," *Appl. Phys. Lett.*, vol. 86, no. 4, pp. 041104-1–041104-5, 2005.

[55] C. Quilliet and B. Berge, "Electrowetting: A recent outbreak," *Current Opinion Colloid Interf. Sci.*, vol. 6, no. 1, pp. 34–39, 2001.

[56] F. Krogmann, W. Monch, A. Werber, and H. Zappe, "Tunable microfluidic micro-lenses," in *The Encyclopedia of Materials: Science and Technology*, K. Buschow, R. Cahn, M. Flemings, P. Veyssiere, E. Kramer, and S. Mahajan, Eds. New York, NY, USA: Pergamon, 2007.

[57] F. Krogmann, W. Monch, and H. Zappe, "A MEMS-based variable micro-lens system," *J. Opt. A, Pure Appl. Opt.*, vol. 8, no. 7, pp. S330–S336, Jul. 2006.

[58] H. Ren and S.-T. Wu, "Tunable-focus liquid microlens array using dielectrophoretic effect," *Opt. Exp.*, vol. 16, no. 4, pp. 2646–2652, 2008.

[59] F. Krogmann, R. Shaik, L. Lasinger, W. Monch, and H. Zappe, "Reconfigurable liquid micro-lenses with high positioning accuracy," *Sens. Actuators A, Phys.*, vol. 143, no. 1, pp. 129–135, 2008.

[60] F. Krogmann, W. Monch, and H. Zappe, "Electrowetting for tunable micro-optics," *J. Microelectromech. Syst.*, vol. 17, pp. 1501–1512, Dec. 2008.

[61] M. Agarwal, R. Gunasekaran, P. Coane, and K. Varahramyan, "Polymer-based variable focal length microlens system," *J. Micromech. Microeng.*, vol. 14, no. 12, pp. 1665–1673, 2004.

[62] A. Werber and H. Zappe, "Tunable microfluidic microlenses," *Appl. Opt.*, vol. 44, no. 16, pp. 3238–3245, Jun. 2005.

[63] W. Zhang, H. Zappe, and A. Seifert, "Polyacrylate membranes for tunable liquid-filled microlenses," *Opt. Eng.*, vol. 52, no. 4, p. 046601, 2013.

[64] D.-Y. Zhang, N. Justis, and Y.-H. Lo, "Fluidic zoom-lens-on-a-chip with wide field-of-view tuning range," *IEEE Photon. Technol. Lett.*, vol. 16, no. 10, pp. 2356–2358, Oct. 2004.

[65] P. Waibel, D. Mader, P. Liebetraut, H. Zappe, and A. Seifert, "Chromatic aberration control for tunable all-silicone membrane microlenses," *Opt. Exp.*, vol. 19, no. 19, pp. 18584–18592, 2011.

[66] P. Müller, A. Kloss, P. Liebetraut, W. Monch, and H. Zappe, "A fully integrated optofluidic attenuator," *J. Micromech. Microeng.*, vol. 21, no. 12, pp. 125027-1–125027-14, 2011.

[67] P. Müller, R. Feuerstein, and H. Zappe, "Integrated optofluidic iris," *J. Microelectromech. Syst.*, vol. 21, no. 5, pp. 1156–1164, Oct. 2012.

[68] H. Choo and R. Muller, "Addressable microlens array to improve dynamic range of Shack–Hartmann sensors," *J. Microelectromech. Syst.*, vol. 15, no. 6, pp. 1555–1567, Dec. 2006.

[69] N. Weber, H. Zappe, and A. Seifert, "A tunable optofluidic silicon optical bench," *J. Microelectromech. Syst.*, vol. 21, no. 6, pp. 1357–1364, Dec. 2012.

[70] N. Weber, D. Hertkorn, H. Zappe, and A. Seifert, "Polymer/silicon hard-magnetic micromirrors," *J. Microelectromech. Syst.*, vol. 21, no. 5, pp. 1098–1106, Oct. 2012.

[71] O. Solgaard, F. S. A. Sandejas, and D. M. Bloom, "A deformable grating optical modulator," *Opt. Lett.*, vol. 17, no. 9, pp. 688–690, May 1992.

[72] A. Godil, "Diffractive MEMS technology offers a new platform for optical network," *Laser Focus World*, vol. 38, no. 5, p. 181, May 2002.

[73] P. M. Hagelin, U. Krishnamoorthy, J. P. Heritage, and O. Solgaard, "Scalable optical cross-connect switch using micromachined mirrors," *IEEE Photon. Technol. Lett.*, vol. 12, no. 7, pp. 882–885, Jul. 2000.

[74] D. M. Marom *et al.*, "Wavelength-selective 1×4 switch for 128 WDM channels at 50 GHz spacing," in *Proc. OFC Conf.*, Mar. 2002, pp. FB7-1–FB7-3.

[75] J.-W. Jeung, S. Vaithilingam, and O. Solgaard, "Frontside-only processing of 2-D MEMS scanner for miniature dual-axis confocal microendoscopes," in *Proc. 16th Int. Conf. Solid-State Sens., Actuators, Microsyst.*, Beijing, China, Jun. 2011, pp. 2908–2911.

[76] D. L. Dickensheets and G. S. Kino, "Micromachined scanning confocal optical microscope," *Opt. Lett.*, vol. 21, no. 10, pp. 764–766, 1996.

[77] S. Kwon, V. Milanovic, and L. P. Lee, "Vertical microlens scanner for 3D imaging," in *Tech. Dig. 2002 Solid-State Sens. Actuator Workshop*, Hilton Head Island, SC, USA, pp. 227–230.

[78] S. Kwon, V. Milanovic, and L. P. Lee, "Vertical combdrive based 2-D gimbaled micromirrors with large static rotation by backside island isolation," *IEEE J. Sel. Topics Quantum Electron.*, vol. 10, no. 3, pp. 498–504, May/Jun. 2004.

[79] S. Kwon and L. P. Lee, "Micromachined transmissive scanning confocal microscope," *Opt. Lett.*, vol. 29, no. 7, pp. 706–708, 2004.

[80] H. Ra, W. Piyawattanametha, Y. Taguchi, D. Lee, M. J. Mandella, and O. Solgaard, "Two-dimensional MEMS scanner for dual-axes confocal microscopy," *J. Micromech. Syst.*, vol. 16, no. 4, pp. 969–976, Aug. 2007.

[81] H. Ra *et al.*, "Three-dimensional in vivo imaging by a handheld dual-axes confocal microscope," *Opt. Exp.*, vol. 16, no. 10, pp. 7224–7232, May 2008.

[82] W. Piyawattanametha *et al.*, "Fast-scanning two-photon fluorescence imaging based on a microelectromechanical systems two-dimensional scanning mirror," *Opt. Lett.*, vol. 31, no. 13, pp. 2018–2020, 2006.

[83] J. Seo, C. L. Kuyper, D. T. Chiu, and P. L. Luke , "Biophotonic MEMS for single molecule detection and manipulation," in *Proc. 2nd Annu. Int. IEEE-EMBS Special Topic Conf. Microtechnol. Med. Biol.*, May 2002, pp. 363–368.

[84] S.-M. Park *et al.*, "Rapid prototyping of nanofluidic systems using size-reduced electrospun nanofibers for biomolecular analysis," *Small*, vol. 6, no. 21, pp. 2420–2426, 2010.

[85] M. J. Levene, J. Korlach, S. W. Turner, M. Foquet, H. G. Craighead, and W. W. Webb, "Zero-mode waveguides for single-molecule analysis at high concentrations," *Science*, vol. 299, no. 5607, pp. 682–686, 2003.

[86] J. M. Moran-Mirabal and H. G. Craighead, "Zero-mode waveguides: Sub-wavelength nanostructures for single molecule studies at high concentrations," *Methods*, vol. 46, no. 1, pp. 11–17, 2008.

[87] J. Eid *et al.*, "Real-time DNA sequencing from single polymerase molecules," *Science*, vol. 323, no. 5910, pp. 133–138, 2009.

[88] D. Psaltis, S. R. Quake, and C. H. Yang, "Developing optofluidic technology through the fusion of microfluidics and optics," *Nature*, vol. 442, no. 7101, pp. 381–386, 2006.

[89] C. Monat, P. Domachuk, and B. J. Eggleton, "Integrated optofluidics: A new river of light," *Nature Photon.*, vol. 1, no. 2, pp. 106–114, 2007.

[90] G. L. Liu, J. Kim, Y. Lu, and L. P. Lee, "Optofluidic control using photothermal nanoparticles," *Nature Mater.*, vol. 5, no. 1, pp. 27–32, 2006.

[91] A. H. J. Yang *et al.*, "Optical manipulation of nanoparticles and biomolecules in sub-wavelength slot waveguides," *Nature*, vol. 457, no. 7225, pp. 71–75, 2009.

[92] V. Lien, Y. Berdichevsky, and Y. H. Lo, "A prealigned process of integrating optical waveguides with microfluidic devices," *IEEE Photon. Technol. Lett.*, vol. 16, no. 6, pp. 1525–1527, Jun. 2004.

[93] S. K. Y. Tang, C. A. Stan, and G. M. Whitesides, "Dynamically reconfigurable liquid-core liquid-cladding lens in a microfluidic channel," *Lab Chip*, vol. 8, no. 3, pp. 395–401, 2008.

[94] X. Q. Cui *et al.*, "Lensless high-resolution on-chip optofluidic microscopes for Caenorhabditis elegans and cell imaging," *Proc. Nat. Acad. Sci. United States Amer.*, vol. 105, no. 31, pp. 10670–10675, 2008.

[95] H. S. Cho, B. Lee, G. L. Liu, A. Agarwal, and L. P. Lee, "Label-free and highly sensitive biomolecular detection using SERS and electrokinetic preconcentration," *Lab Chip*, vol. 9, no. 23, pp. 3360–3363, 2009.

[96] D. Choi, T. Kang, H. Cho, Y. Choi, and L. P. Lee, "Additional amplifications of SERS via an optofluidic CD-based platform," *Lab Chip*, vol. 9, no. 2, pp. 239–243, 2009.

[97] S.-M. Park, Y. S. Huh, H. G. Craighead, and D. Erickson, "A method for nanofluidic device prototyping using elastomeric collapse," *Proc. Nat. Acad. Sci. United States Amer.*, vol. 106, no. 37, pp. 15549–15554, 2009.

[98] M. Lee, K. Lee, K. H. Kim, K. W. Oh, and J. Choo, "SERS-based immunoassay using a gold array-embedded gradient microfluidic chip," *Lab Chip*, vol. 12, no. 19, pp. 3720–3727, 2012.

[99] S. E. Chung *et al.*, "Optofluidic maskless lithography system for real-time synthesis of photopolymerized microstructures in microfluidic channels," *Appl. Phys. Lett.*, vol. 91, no. 4, p. 041106, 2007.

[100] S. A. Lee, S. E. Chung, W. Park, S. H. Lee, and S. Kwon, "Three-dimensional fabrication of heterogeneous microstructures using soft membrane deformation and optofluidic maskless lithography," *Lab Chip*, vol. 9, no. 12, pp. 1670–1675, 2009.

[101] C. Grillet *et al.*, "Reconfigurable photonic crystal circuits," *Laser Photon. Rev.*, vol. 4, no. 2, pp. 192–204, 2010.

[102] C. Karnutsch *et al.*, "Temperature stabilization of optofluidic photonic crystal cavities," *Appl. Phys. Lett.*, vol. 94, no. 23, p. 231114, 2009.

[103] U. Bog *et al.*, "High-Q microfluidic cavities in silicon-based two-dimensional photonic crystal structures," *Opt. Lett.*, vol. 33, no. 19, pp. 2206–2208, 2008.

[104] K. Yu and O. Solgaard, "Tunable optical transversal filters based on a Gires–Tournois interferometer with MEMS phase shifters," *IEEE J. Sel. Topics Quantum Electron.*, vol. 10, no. 3, pp. 588–597, May/Jun. 2004.

[105] A. F. Sarioglu, M. Lui, and O. Solgaard, "High resolution nanomechanical mapping using interferometric-force-sensing AFM probes," *J. Microelectromech. Syst.*, vol. 20, no. 3, pp. 654–664, Jun. 2011.

[106] K. Vijayraghavan, A. A. Gellineau, A. Wang, M. J. Butte, N. A. Melosh, and O. Solgaard, "High-bandwidth AFM probes for imaging in air and fluid," *J. Microelectromech. Syst.*, vol. 22, no. 3, pp. 603–612, Jun. 2013.

[107] K. Vijayraghavan, A. Wang, O. Solgaard, M. J. Butte, and N. A. Melosh, "Measurement of elastic properties in fluid using high bandwidth atomic force microscope probes," *Appl. Phys. Lett.*, vol. 102, no. 10, p. 103111, 2013.

[108] R. St-Gelais, A. Poulin, and Y.-A. Peter, "Advances in modeling, design, and fabrication of deep-etched multilayer resonators," *J. Lightw. Technol.*, vol. 30, no. 12, pp. 1900–1908, Jun. 15, 2012.

[109] J. Masson, R. St-Gelais, A. Poulin, and Y.-A. Peter, "Tunable fiber laser using a MEMS-based in plane Fabry–Pérot filter," *IEEE J. Quantum Electron.*, vol. 46, no. 9, pp. 1313–1319, Sep. 2010.

[110] R. St-Gelais, J. Masson, and Y.-A. Peter, "All-silicon integrated Fabry–Pérot cavity for volume refractive index measurement in microfluidic systems," *Appl. Phys. Lett.*, vol. 94, no. 24, p. 243905, 2009.

[111] K. Zandi, J. A. Bélanger, and Y.-A. Peter, "Design and demonstration of an in-plane silicon-on-insulator optical MEMS Fabry–Pérot-based accelerometer integrated with channel waveguides," *J. Microelectromech. Syst.*, vol. 21, no. 6, pp. 1464–1470, Dec. 2012.

[112] R. St-Gelais *et al.*, "Gas sensing using polymer-functionalized deformable Fabry–Pérot interferometers," *Sens. Actuators B, Chem.*, vol. 182, pp. 45–52, Jun. 2013.

[113] M. Malak, F. Marty, N. Pavy, Y.-A. Peter, A.-Q. Liu, and T. Bourouina, "Cylindrical surfaces enable wavelength-selective extinction and sub-0.2 nm linewidth in 250 μm-gap silicon Fabry–Pérot cavities," *J. Microelectromech. Syst.*, vol. 21, no. 1, pp. 171–180, Feb. 2012.

[114] A. Poulin, R. St-Gelais, N. Goulamhoussen, G. Zhu, C. Boudoux, and Y.-A. Peter, "In-plane MEMS-based Fabry–Pérot filter for high-speed wavelength-swept semiconductor laser," in *Proc. Solid-State Sens., Actuators, Microsyst. Workshop*, Hilton Head Island, SC, USA, 2012, pp. 401–404.

[115] A. Leblanc-Hotte, R. St-Gelais, and Y.-A. Peter, "Optofluidic device for high resolution volume refractive index measurement of single cell," in *Proc. 6th Int. Conf. Miniaturized Syst. Chem. Life Sci.*, Okinawa, Japan, 2012, pp. 1330–1332.

[116] A. Leblanc-Hotte, J.-S. Delisle, S. Lesage, and Y.-A. Peter, "Optofluidic device for high resolution and multiparametric measurement of single biological cells," in *Proc. Solid-State Sens., Actuators, Microsyst. Workshop*, Hilton Head Island, SC, USA, 2014.

[117] X. J. Liang, A. Q. Liu, C. S. Lim, T. C. Ayi, and P. H. Yap, "Determining refractive index of single living cell using an integrated microchip," *Sens. Actuators A, Phys.*, vol. 133, no. 2, pp. 349–354, 2007.

[118] K. Vahala, "Optical microcavities," *Nature*, vol. 424, pp. 839–846, Aug. 2003.

[119] S. Noda, M. Fujita, and T. Asano, "Spontaneous-emission control by photonic crystals and nanocavities," *Nature Photon.*, vol. 1, no. 8, pp. 449–458, 2007.

[120] F. Vanier, M. Rochette, N. Godbout, and Y.-A. Peter, "Raman lasing in As_2S_3 high-Q whispering gallery mode resonators," *Opt. Lett.*, vol. 38, no. 23, pp. 4966–4969, 2013.

[121] S. Bergeron, S. Saïdi, and Y.-A. Peter, "Periodic and non-periodic frequency selection in an erbium doped fiber laser by silica microdisk optical cavity filters," *Opt. Exp.*, vol. 18, no. 16, pp. 16797–16804, 2010.

[122] A. M. Armani, R. P. Kulkarni, S. E. Fraser, R. C. Flagan, and K. J. Vahala, "Label-free, single-molecule detection with optical microcavities," *Science*, vol. 317, no. 5839, pp. 783–787, 2007.

[123] F. Vollmer and S. Arnold, "Whispering-gallery-mode biosensing: Label-free detection down to single molecules," *Nature Methods*, vol. 5, no. 7, pp. 591–596, 2008.

[124] T. J. Kippenberg, R. Holzwarth, and S. A. Diddams, "Microresonator-based optical frequency combs," *Science*, vol. 332, no. 6029, pp. 555–559, 2011.

[125] T. J. Kippenberg and K. J. Vahala, "Cavity optomechanics: Back-action at the mesoscale," *Science*, vol. 321, no. 5893, pp. 1172–1176, 2008.

[126] M. Eichenfield, R. Camacho, J. Chan, K. J. Vahala, and O. Painter, "A picogram- and nanometre-scale photonic-crystal optomechanical cavity," *Nature*, vol. 459, no. 7246, pp. 550–555, 2009.

[127] E. M. Purcell, "Spontaneous emission probabilities at radio frequencies," *Phys. Rev.*, vol. 69, nos. 1–2, p. 681, 1946.

[128] L. Shi, P. Pottier, Y.-A. Peter, and M. Skorobogatiy, "Guided-mode resonance photonic crystal slab sensors based on bead monolayer geometry," *Opt. Exp.*, vol. 16, no. 22, pp. 17962–17971, 2008.

[129] N. Ganesh *et al.*, "Enhanced fluorescence emission from quantum dots on a photonic crystal surface," *Nature Nanotechnol.*, vol. 2, no. 8, pp. 515–520, 2007.

[130] O. Kilic *et al.*, "Photonic crystal slabs demonstrating strong broadband suppression of transmission in the presence of disorders," *Opt. Lett.*, vol. 29, no. 23, pp. 2782–2784, 2004.

[131] W. Suh, M. F. Yanik, O. Solgaard, and S. Fan, "Displacement-sensitive photonic crystal structures based on guided resonance in photonic crystal slabs," *Appl. Phys. Lett.*, vol. 82, no. 13, pp. 1999–2001, 2003.

[132] L. Shi, P. Pottier, M. Skorobogatiy, and Y.-A. Peter, "Tunable structures comprising two photonic crystal slabs–optical study in view of multi-analyte enhanced detection," *Opt. Exp.*, vol. 17, no. 13, pp. 10623–10632, 2009.

[133] J. Jeong, B. Park, H. Keum, S. Kim, J. Rogers, and O. Solgaard, "Two-axis MEMS scanner with transfer-printed high-reflectivity, broadband monolithic silicon photonic crystal mirrors," *Opt. Exp.*, vol. 21, no. 11, pp. 13800–13809, 2013.

[134] S. Fan and J. D. Joannopoulos, "Analysis of guided resonances in photonic crystal slabs," *Phys. Rev. B*, vol. 65, no. 23, p. 235112, 2002.

[135] C. Chase, Y. Rao, W. Hofmann, and C.-J. Chang-Hasnain, "1550 nm high contrast grating VCSEL," *Opt. Exp.*, vol. 18, no. 15, pp. 15461–15466, 2010.

[136] W. Suh, M. F. Yanik, O. Solgaard, and S.-H. Fan, "Displacement-sensitive photonic crystal structures based on guided resonance in photonic crystal slabs," *Appl. Phys. Lett.*, vol. 82, no. 13, pp. 1999–2001, Mar. 2003.

[137] V. Lousse, W. Suh, O. Kilic, S. Kim, O. Solgaard, and S. Fan, "Angular and polarization properties of a photonic crystal slab mirror," *Opt. Exp.*, vol. 12, no. 8, pp. 1575–1582, Apr. 2004.

[138] O. Kilic, S. Fan, and O. Solgaard, "Analysis of guided-resonance-based polarization beam splitting in photonic crystal slabs," *J. Opt. Soc. Amer. A*, vol. 25, no. 11, pp. 2680–2692, Nov. 2008.

[139] W. Suh and S. Fan, "Mechanically switchable photonic crystal filter with either all-pass transmission or flat-top reflection characteristics," *Opt. Lett.*, vol. 28, no. 19, pp. 1763–1765, 2003.

[140] B. Park, J. Provine, I.-W. Jung, R. T. Howe, and O. Solgaard, "Photonic crystal fiber tip sensor for high-temperature measurement," *IEEE Sensors J.*, vol. 11, no. 11, pp. 2643–2648, Nov. 2011.
[141] I.-W. Jung, B. Park, J. Provine, R. T. Howe, and O. Solgaard, "Highly sensitive monolithic silicon photonic crystal fiber tip sensor for simultaneous measurement of refractive index and temperature," *J. Lightw. Technol.*, vol. 29, no. 9, pp. 1367–1374, May 1, 2011.
[142] J. O. Grepstad, P. Kaspar, O. Solgaard, I.-R. Johansen, and A. S. Sudbø, "Photonic-crystal membranes for optical detection of single nanoparticles, designed for biosensor application," *Opt. Exp.*, vol. 20, no. 7, pp. 7954–7965, Mar. 2012.
[143] S. Hadzialic, S. Kim, A. S. Sudbo, and O. Solgaard, "Two-dimensional photonic crystals fabricated in monolithic single-crystal silicon," *IEEE Photon. Technol. Lett.*, vol. 22, no. 2, pp. 67–69, Jan. 15, 2010.
[144] S. B. Mallick, I.-W. Jung, A. M. Meisner, J. Provine, R. T. Howe, and O. Solgaard, "Multilayered monolithic silicon photonic crystals," *IEEE Photon. Technol. Lett.*, vol. 23, no. 11, pp. 730–732, Jun. 1, 2011.
[145] I. W. Jung, S. B. Mallick, and O. Solgaard, "A large-area high-reflectivity broadband monolithic single-crystal-silicon photonic crystal MEMS scanner with low dependence on incident angle and polarization," *IEEE J. Sel. Topics Quantum Electron.*, vol. 15, no. 5, pp. 1447–1454, Sep./Oct. 2009.
[146] O. C. Akkaya, O. Kilic, M. J. F. Digonnet, G. S. Kino, and O. Solgaard, "Modeling and demonstration of thermally stable high-sensitivity reproducible acoustic sensors," *J. Microelectromech. Syst.*, vol. 21, no. 6, pp. 1347–1356, Dec. 2012.
[147] X. Wu, C. Jan, and O. Solgaard, "Monolithic photonic crystal-based fiber-tip Fabry–Pérot static pressure sensor," in *Proc. 2013 Int. Conf. Optical MEMS Nanophoton.*, Kanazawa, Japan, Aug., pp. 49–50.
[148] I. S. Grudinin, V. S. Ilchenko, and L. Maleki, "Ultrahigh optical Q factors of crystalline resonators in the linear regime," *Phys. Rev. A*, vol. 74, no. 6, p. 063806, 2006.
[149] H. Lee *et al.*, "Chemically etched ultrahigh-Q wedge-resonator on a silicon chip," *Nature Photon.*, vol. 6, no. 6, pp. 369–373, 2012.
[150] F. Vanier, C. L. Mela, A. Hayat, and Y.-A. Peter, "Intrinsic quality factor determination in whispering gallery mode microcavities using a single Stokes parameters measurement," *Opt. Exp.*, vol. 19, no. 23, pp. 23544–23553, 2011.
[151] A. M. Armani, R. P. Kulkarni, S. E. Fraser, R. C. Flagan, and K. J. Vahala, "Label-free, single-molecule detection with optical microcavities," *Science*, vol. 317, no. 5839, pp. 783–787, 2007.
[152] F. Vollmer and S. Arnold, "Whispering-gallery-mode biosensing: Label-free detection down to single molecules," *Nature Methods*, vol. 5, no. 7, pp. 591–596, 2008.
[153] T. J. Kippenberg, R. Holzwarth, and S. A. Diddams, "Microresonator-based optical frequency combs," *Science*, vol. 332, no. 6029, pp. 555–559, 2011.
[154] T. J. Kippenberg and K. J. Vahala, "Cavity optomechanics: Back-action at the mesoscale," *Science*, vol. 321, no. 5893, pp. 1172–1176, 2008.
[155] S. Bergeron, F. Vanier, and Y.-A. Peter, "Silica microdisk coupled resonator optical waveguide," in *Proc. IEEE/LEOS Int. Conf. Optical MEMS Nanophoton.*, Clearwater, FL, USA, Aug. 2009, pp. 73–74.
[156] F. Vanier, M. Rochette, and Y.-A. Peter, "Raman scattering emission in high Q factor As_2S_3 microspheres," in *Proc. CLEO*, San Jose, CA, USA, 2013, no. CM1L.8.

Olav Solgaard earned his Ph.D. degree from Stanford University in 1992. His doctoral dissertation, "Integrated Semiconductor Light Modulators for Fiber-optic and Display Applications," was the basis for the establishment of a Silicon Valley firm Silicon Light Machines (SLM), co-founded by Dr. Solgaard in 1994. From 1992 to 1995 he carried out research on optical MEMS as a Postdoctoral Fellow at the University of California, Berkeley, and in 1995, he joined the Electrical Engineering faculty of the University of California, Davis. In 1999 he joined Stanford University where he is now a Professor of Electrical Engineering and the Director of the Edward L. Ginzton Laboratory. Professor Solgaard's research interests include optical MEMS, Photonic Crystals, optical sensors, microendoscopy, atomic force microscopy, and solar energy conversion. He has authored more than 350 technical publications and holds 60 patents. Professor Solgaard came to Stanford with the support of a Royal Norwegian Council for Scientific and Industrial Research Fellowship in 1986 and was named a Terman Fellow at Stanford for the period 1999-2002. He is a Fellow of the Optical Society of America, the Royal Norwegian Society of Sciences and Letters, and the Norwegian Academy of Technological Sciences.

Asif A. Godil is the President/CEO of AG Microsystems (AGM), a leading company in the Optical MEMS space for Optical Telecom Networks, which he founded in 2005. Prior to his work at AGM, Asif founded and built LIGHTCONNECT, a Venture Capital funded startup, into a major supplier of MEMS-based fiber optic components and modules for the Telecom market. In June 2006, LIGHTCONNECT was successfully acquired by Neophotonics Corporation. In the Optical MEMS space, a highly significant development was the GLV (Grating Light Valve) based scanned projection display, which Asif co-invented and developed at Silicon Light Machines, the company where he worked prior to LIGHTCONNECT. Silicon Light Machines was later acquired by Cypress Semiconductor, and the GLV based display technology was licensed to Sony Corporation. After Asif completed his Ph.D. from Stanford University, Sony invited him to spend a couple of years as a Visiting Scientist at its Research Center in Tokyo, Japan. Asif has a Bachelor's degree in Electrical Engineering from the University of Delaware, and a Ph.D. in Electrical Engineering from Stanford University.

Roger T. Howe (S'80–M'84–SM'93–F'96) is the William E. Ayer Professor in the Department of Electrical Engineering at Stanford University. He received a B.S. degree in physics from Harvey Mudd College, and an M.S. and Ph.D. in electrical engineering from the University of California, Berkeley, in 1981 and 1984. After faculty positions at Carnegie-Mellon University and MIT from 1984-1987, he returned to UC Berkeley where he was a Professor until 2005.

His research interests include microelectromechanical system design, micro- and nano-machining technologies, and applications in energy conversion and biomolecular sensing.

Prof. Howe served as Co-General Chair of the IEEE MEMS'90 Workshop in Napa, California, and was the Technical Program Chair of Transducers '03 in Boston. He is an editor of the IEEE/ASME JOURNAL OF MICROELECTROMECHANICAL SYSTEMS. He was co-recipient of the 1998 IEEE Cledo Brunetti Award, and was elected to the U.S. National Academy of Engineering in 2005 for his contributions to MEMS processes, devices, and systems. He co-founded Silicon Clocks, Inc., a start-up company commercializing integrated MEMS resonator-based timing products, which was acquired in April 2010 by Silicon Laboratories, Inc. In December 2010, he became the Faculty Director of the Stanford Nanofabrication Facility (SNF) and in September 2011, he became Director of the National Nanotechnology Infrastructure Network (NNIN), which is an NSF-funded collaboration of 14 academic nanofabrication facilities across the U.S.

Luke P. Lee is an Arnold and Barbara Silverman Distinguished Professor of Bioengineering, Electrical Engineering and Computer Science, and Biophysics at UC Berkeley. He is Co-Director of the Berkeley Sensor and Actuator Center. He received both his BA in Biophysics, and PhD in Applied Physics (major) and Bioengineering (minor) from UC Berkeley. He joined the faculty at the UC Berkeley in 1999, and then became the Lester John and Lynne Dewar Lloyd Distinguished Professor of Bioengineering and Professor of Biophysics at Berkeley in 2005. He also served as the Chair Professor in Systems Nanobiology at the Swiss Federal Institute of Technology (ETH, Zürich) from 2006 to 2007. His work at the interface of biological, physical, and engineering sciences for medicine has been recognized by many honors that include the IEEE William J. Morlock Award, NSF Career Award, Fulbright Scholar Award, and the HoAm Prize. He is a Fellow of the Royal Society of Chemistry and the American Institute of Medical and Biological Engineering (AIMBE). His current research interests are nanoscale biophotonics in living cells, molecular diagnostics of infectious and neurodegenerative diseases, bioinspired neural interfaces and organs on a chip, and *in vitro* neurogenesis, with a focus both on studying fundamental quantum nanobiology and on solving ill-defined problems of healthcare.

Yves-Alain Peter (S'93–M'03–SM'07) received the M.Sc. degree in physics and the Dr.Sc. degree in sciences from the University of Neuchâtel, Switzerland, in 1994 and 2001, respectively.

In 1995, he was a Research Associate with the Department of Medical Radiobiology, Paul Scherrer Institute, Switzerland. From 1995 to 2001, he was a Graduate Research Assistant with the Applied Optics Group, Institute of Microtechnology, University of Neuchâtel. From 2001 to 2003, he was a Post-Doctoral Researcher with the Microphotonics Group, Stanford University. From 2003 to 2004, he was a Research and Development Engineer and a Project Leader with the Swiss Center for Electronics and Microtechnology, Switzerland. In 2004, he joined Polytechnique Montréal, Canada, where he is now Professor of Engineering Physics. His current research interests include microphotonics and microoptoelectromechanical systems.

Hans Zappe is the Gisela and Erwin Sick Professor of Micro-optics in the Department of Microsystems Engineering at the University of Freiburg, Germany. Born in France and raised in New York, he earned his Bachelor's and Master's degrees at MIT and his PhD from the University of California, Berkeley, all in Electrical Engineering. After pursuing research activities in electronics, integrated optics and semiconductor lasers at IBM, the Fraunhofer Institute for Applied Solid State Physics and the Centre Suisse d'Electronique et de Microtechnique, he joined the University of Freiburg in 2000, where he was Dean of Engineering from 2008 to 2010. His current research interests focus on tunable micro-optics, optical micro-systems for medical applications and printable micro-optics.